

# Towards Unsupervised Domain Adaptation via Domain-Transformer

Chuan-Xian Ren, Yi-Ming Zhai, You-Wei Luo and Meng-Xue Li

**Abstract**—As a vital problem in pattern analysis and machine intelligence, Unsupervised Domain Adaptation (UDA) studies how to transfer an effective feature learner from a labeled source domain to an unlabeled target domain. Plenty of methods based on Convolutional Neural Networks (CNNs) have achieved promising results in the past decades. Inspired by the success of Transformers, some methods attempt to tackle UDA problem by adopting pure transformer architectures, and interpret the models by applying the long-range dependency strategy at image patch-level. However, the algorithmic complexity is high and the interpretability seems weak. In this paper, we propose the Domain-Transformer (DoT) for UDA, which integrates the CNN-backbones and the core attention mechanism of Transformers from a new perspective. Specifically, a plug-and-play domain-level attention mechanism is proposed to learn the sample correspondence between domains. This is significantly different from existing methods which only capture the local interactions among image patches. Instead of explicitly modeling the distribution discrepancy from either domain-level or class-level, DoT learns transferable features by achieving the local semantic consistency across domains, where the domain-level attention and manifold regularization are explored. Then, DoT is free of pseudo-labels and explicit domain discrepancy optimization. Theoretically, DoT is connected with the optimal transportation algorithm and statistical learning theory. The connection provides a new insight to understand the core component of Transformers. Extensive experiments on several benchmark datasets validate the effectiveness of DoT.

**Index Terms**—Feature learning, Domain adaptation, Discriminative analysis, Attention, Sample correspondence.

## 1 INTRODUCTION

It is well-known that deep learning methods have achieved remarkable progress on various computer vision and pattern recognition tasks, and the progress is highly dependent on large-scale labeled datasets and the identical distribution assumption. However, data collected from the real-world scenarios are usually unlabeled, and manual annotation is always expensive and time-consuming. Moreover, there exists a large distribution gap since the training set and the test set may be collected with different visual conditions, such as sensors, backgrounds and views. To deal with the shortage of labeled data, a natural idea is transferring the knowledge from a label-rich domain (i.e., source domain) to a label-scarce domain (i.e., target domain). This is usually called Unsupervised Domain Adaptation (UDA) problem [1], [2], [3], [4], [5].

Generally, with the labeled source samples, UDA-oriented methods attempt to learn flexible feature representations that can generalize well to the unlabeled target domain. As shown in Figure 1, UDA methods can tackle the generalization problem by exploiting the distribution approximation or point set matching manners. The most common setting of UDA is that the feature spaces between source and target domains are the same but the marginal distributions are different, i.e.,  $P_X^s \neq P_X^t$ . The rigorous transfer theory [6] shows that the classifier's target error is mainly bounded by its source error plus the divergence between the two domains. Under the guidance of this theory, a major line of methods are designed to learn domain-

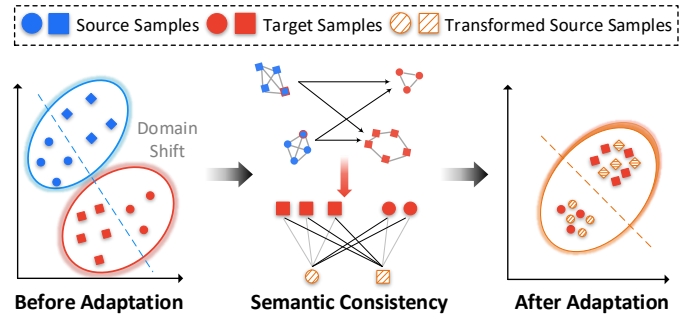


Fig. 1. The primary goal of UDA is to generalize the classifier trained on the source domain to the unlabeled target domain. Direct application of the learned classifier suffered from the “domain shift” problem (left). UDA methods try to learn semantic consistency across domains (middle) and then reduce the mis-classification rate on the target domain (right).

invariant features by simultaneously minimizing the source error and some statistical discrepancies between domain distributions, e.g., Maximum Mean Discrepancy (MMD) [7], [3], statistic moment matching [8], manifold alignment [9], [5] and adversarial domain adaptation [10], [11], [12]. Additionally, another fruitful line is based on Optimal Transportation (OT) [13], [14], [15], which matches the marginal distributions by mapping samples from the source domain to the target domain with an optimal transportation plan  $\gamma$ . With the marginal distribution constraints on  $\gamma$ , OT-based methods learn transferable features by achieving a pair-wise matching between samples across domains.

Extended from mitigating domain distribution discrepancy based on the marginal shift assumption, domain alignment with semantic consistency, as shown in Figure 1, is studied recently based on the conditional shift assumption [16], i.e.,  $P_{X|Y}^s \neq P_{X|Y}^t$ . Combes *et al.* [17] provide an inter-

C.-X. Ren, Y.-M. Zhai and Y.-W. Luo are with the School of Mathematics, Sun Yat-Sen University, Guangzhou, 510275, China. M.-X. Li is with Alibaba Group, Hangzhou, 311100, China. C.-X. Ren is the corresponding author (email: rchuanx@mail.sysu.edu.cn).

pretable generalization bound, which shows that reducing conditional shift is necessary in UDA. There are several works explore the semantic consistency of domains by matching conditional and even joint distributions, *e.g.*, extensions of MMD [18], [19], conditional adversarial adaptation [20], centroid alignment [4], OT-based joint distribution matching [21], [14], and conditional statistic alignment [22]. It is worth noting that most of these methods rely on the pseudo-labels of the target samples since the target domain is unlabeled. False predictions on the pseudo-labels are expected to be iteratively corrected in the training process. However, to obtain reliable pseudo-labels, the procedure may be associated with several hyper-parameters and elaborately designed threshold values. These phases introduce extra risk and complexity in model training. Thus, how to effectively learn semantic consistency is still fundamental and challenging in dealing with UDA problem.

The Transformer [23] has achieved immense success in natural language process due to its key introduction of the attention mechanism, which has a strong ability on modeling long-range dependency and semantic information in sequences. The evolution of Transformers has sparked a rising interest in applying them to computer vision. Vision Transformer (ViT) [24] is the first proposal to replace backbone of CNNs [25] with a pure Transformer model, which has achieved state-of-the-art performance in many image classification tasks. A series of variants, *e.g.*, Data-efficient image Transformer (DeiT) [26], Pyramid Vision Transformer (PVT) [27] and Swin Transformer (Swin) [28], further improve the performance from different perspectives.

The attention mechanism in Transformers can be roughly categorized into two groups, namely, self-attention and cross-attention, which are employed in the encoder module and decoder module, respectively. The queries and key-value pairs of the self-attention mechanism come from the same place, but different places for the cross-attention. The cross-attention mechanism can be employed for feature fusion [29], [30]. Different from the CNN-backbones, which just focus on local characteristics by using convolutional filters [31], the visual Transformers can capture global information between patches for each image sample. Though different Transformer architectures have shown great potential in visual tasks, the final performance still rely heavily on large-scale datasets and sufficient computing resources for training. Additionally, it seems that few works pay attention to the interpretability of attention at the domain-level and its real performance on domain-adaptive feature extraction.

In this paper, instead of employing a pure transformer-based feature extractor, we propose a novel model called Domain-Transformer (DoT) for UDA, which mainly consists of three parts, *i.e.*, the feature extractor based on CNN-backbones, the domain-level attention and the shared classifier. Different from most visual Transformers, which directly utilize the attention mechanism at *patch-level* to capture the object region, we capture the correspondence of samples across domains by proposing the cross-attention mechanism at *domain-level*. The domain-level attention can serve as a plug-and-play module for existing UDA methods. One the one hand, the domain-level attention is closely related to the optimal transport theory, and then the DoT model can be interpreted by the generalization error in

learning theory. On the other hand, DoT is able to learn more transferable features by mapping the source samples onto the target domain through the domain-level attention. It is worth noting that the transformed source samples are essentially weighted by target samples with the same class labels, because larger weights are usually obtained by the within-class samples. Thus, the classifier trained with the transformed source samples will fit the target domain well. In order to obtain the transformed source samples with more relevant target samples, we employ the local structure learning phase to make sure that samples within the same class keep nearby in the latent space. The domain-level attention and the local structure learning phase are highly interrelated, and their integration plays an important role in matching the local structures across domains.

To the best of our knowledge, DoT is the first effort to achieve local semantic consistency at class-level by incorporating the merits of the CNN-backbones and the domain-level attention simultaneously. The contributions of our work are summarized as follows.

- 1) Instead of explicitly modeling the domain discrepancy, DoT formulates the long-range dependency across domains and learns shared features for knowledge transfer, which ensure the local semantic consistency. Besides, different from most visual transformers capturing interactions at patch-level, DoT models the sample correspondence at domain-level.
- 2) The domain-level attention mechanism is theoretically connected with the OT framework. The long-range dependency across domains is mathematically analogous to the transport map in OT. Thus, DoT provides new insight to the inherency of both Transformers and domain-adaptive feature learning.
- 3) From the perspective of learning theory, an informative generalization bound is derived based on Wasserstein OT geometry. It bridges the gap between the domain-level attention mechanism and generalization error in UDA, and ensures that DoT is sufficient for learning transferable features..
- 4) DoT is free of pseudo-labels in the target domain, which avoids the uncertainty in pseudo-labeling procedure, and it can be optimized in an end-to-end manner. Extensive experiment results validate the effectiveness of DoT on tackling UDA problem.

The rest of this paper is organized as follows. In Section 2, we present a brief review of related UDA methods and the vision-oriented Transformers. Section 3 depicts the DoT method in details. Extensive experimental results and analysis on several benchmark datasets are presented in Section 4, which is followed by conclusions and future works in Section 5.

## 2 RELATED WORK

In this section, some pioneering works on UDA and visual Transformers are briefly reviewed.

### 2.1 Unsupervised Domain Adaptation

UDA aims to generalize an effective feature learner with semantic consistency, which is trained on the labeled source

domain, to the unlabeled target domain. The source and target domains have similar but not identical distributions. Most existing methods focus on the domain alignment by minimizing various metrics. The related literature can be roughly categorized into two groups, i.e., moment matching-based methods and adversarial training-based methods. The statistic moment matching methods attempt to mitigate the domain discrepancy by aligning the statistics of the source and target distributions, e.g., MMD based methods Transfer Component Analysis (TCA) [7] and Domain Adaptation Network (DAN) [3], and covariance based methods CORrelation ALignment (CORAL) [8]. Luo *et al.* [5] propose a Discriminative Manifold Propagation (DMP) method based on manifold metrics to bridge the source and target distributions, which generalizes Fisher’s discriminant criterion [32] by exploiting the between-class scatter in the source domain and the within-class scatter in the target domain. The adversarial training-based methods provide a discriminator to distinguish the source domain and the target domain. Ganin *et al.* [10] provide Domain Adversarial Neural Networks (DANN) to learn deep features, which minimizes the loss of the category classifier and maximizes the loss of the domain classifier. Extended from minimizing the domain discrepancy at a domain-level, more and more works make effort on learning more discriminative domain-invariant features by conditioning the label information [4], [18], [20], [33], [34]. Long *et al.* [20] define a novel domain discriminator conditioned on the classifier predictions in Conditional Domain Adversarial Network (CDAN). Pan *et al.* [35] propose a Transferable Prototypical Network (TPN), which minimizes the distances between prototypes of the source domain with labels and target domain with pseudo-labels. Zhu *et al.* [34] provide a local maximum mean discrepancy, then match the distributions of relevant subdomains by proposing a Deep Subdomain Adaptation Network (DSAN). Yang *et al.* [4] propose a graph attention network which transfers the semantic information by aligning the class-wise centroids.

Recently, OT has been successfully applied to UDA problem, and it has strong theoretical foundation in graph theory and mathematical optimization. Courty *et al.* [2] aim to realize domain alignment by solving the optimal transport plan of an entropy-regularized OT model. Zhang *et al.* [13] provide a theoretical and framework of OT in reproducing kernel Hilbert spaces (RKHS), then address the distribution matching problem by using kernel-based transport map. These OT-based methods tend to align domains through a pair-wise matching between samples across domains, however, they ignore the real influence of label information. To make full use of the label-based locality structure, Courty *et al.* [21] propose the Joint Distribution Optimal Transport (JDOT) and Damodaran *et al.* [14] extend it to the deep learning framework as DeepJDOT. They are the first attempt to seek the optimal classifier for the target domain by minimizing the optimal transport distance between the joint distributions. Technically, it uses the total distance with the deep features and label vectors, respectively. Li *et al.* propose an Enhanced Transport Distance (ETD) method [15], which reweighs the transport distance with the similarity between feature vectors from different domains. Inspired by the kernel Bures metric studied in [13], Luo *et al.* propose the

Conditional Kernel Bures (CKB) metric [22] for characterizing the class-wise domain discrepancy.

Compared with current UDA models, DoT learns the semantic consistency without inducing explicit domain discrepancy optimization and pseudo-label procedure, which ensures smaller estimation risk and computation complexity. Besides, DoT can be theoretically connected with the OT algorithm, which guarantees the interpretability of model.

## 2.2 Transformers for Vision

The standard Transformer [23] and its various variants [36], [24], [28] are built upon the attention mechanism, which maps a query  $q$  and a set of key-value pairs  $(k, v)$  to formulate a series of matching probabilistic weights. The probabilistic weight assigned to each value depends on the similarity between the query and the corresponding key. To extend the Transformers to images-based learning tasks, vision Transformers [24], [28] usually split each image into  $N$  patches, which are then formulated as feature matrix  $Z \in \mathbb{R}^{N \times D}$ . Suppose  $Q, K$  and  $V \in \mathbb{R}^{N \times D_h}$ , the attention mechanism, which is essentially in the encoder module of the Transformer, is formulated as

$$A = \text{Softmax} \left( \frac{QK^T}{\sqrt{D_h}} \right) \in \mathbb{R}^{N \times N},$$

Then, the attention values of  $Z$  is characterized by

$$\text{Attention}(Z) = AV.$$

This attention builds the long-range dependency among patches of each image, which allows Transformer to identify the image regions semantically relevant to classification.

In Transformers, all the queries  $q$ , keys  $k$  and values  $v$  for the attention mechanism come from the same feature matrix  $Z$  but with different projections. This kind of attention is also named as self-attention. Obviously, queries and the set of key-value pairs are not required to be from the same place [37], [38], and this leads to the cross-attention mechanism. Note that the real performance of the pure Transformers relies heavily on labeled large-scaled datasets and sufficient computing resource for model training [24]. Fortunately, there are more and more researchers improving the Transformer-based models and applying them to a wider range of visual tasks. ViT [24] addresses the image classification task by directly applying the pure Transformer model on the sequence of patch embeddings. Actually, It only adopts the encoder part of the Transformer. DeiT [26] introduces a teacher-student strategy that relies on a distillation token to ViT. PVT [27] achieves dense prediction tasks by introducing the pyramid structure into Transformer. Swin [28] uses a hierarchical transformer architecture to model representations at various scales. Generally, the attention mechanism in most models are used to integrate relevant information among patches within the same image or between two different images.

To identify transferable image regions, Wang *et al.* [39] present Transferable Attention for Domain Adaptation (TADA), where the global attention is generated by sample-based domain discriminator and the local attention is generated by patch-based domain discriminator. Ma *et al.* propose the Win-Win Transformer (WinTR) [40] to exploit

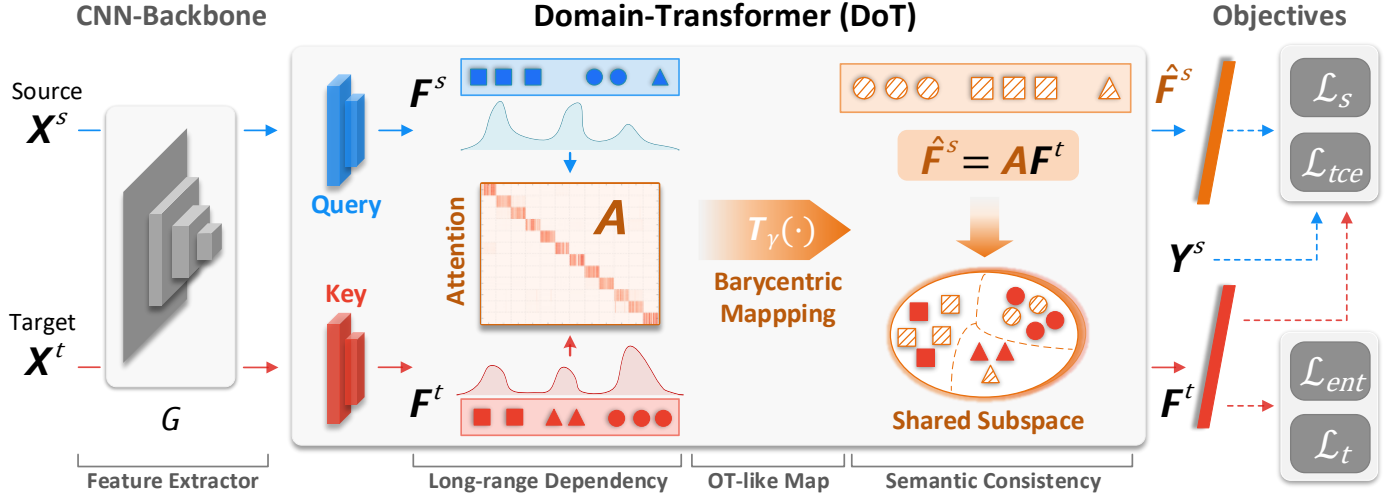


Fig. 2. Schematic illustration of our method, which consists of three parts, i.e., the shared CNN-backbone, the domain-transformer (DoT) and the shared classifier. In particular, DoT can be further decomposed into the long-range dependency characterization, the OT-like map and the semantic consistency learning phases. It essentially explores the *sample correspondence between domains* by using the novel attention mechanism at domain-level. With the projection from the source (e.g.,  $F^s$ ) onto the subspace of target domain, the new feature vectors (e.g.,  $\hat{F}^s$ ) are weighted by the most relevant ones in the target domain, and thus, they are expected to be transferable and adaptive across domains. Best viewed in color.

both domain-specific and invariant knowledge. The cross-domain knowledge is transferred via source-guided label refinement and single-sided feature alignment with respect to source or target. To exploit the transferability of vision Transformer for domain adaptation, Yang *et al.* [41] propose Transferable Vision Transformer (TVT) by applying an adversarial discriminator to the class tokens. Yang *et al.* [42] consider the source-free domain adaptation task, and they propose the Transformer-based Domain Adaptation (TransDA) method to focus on object regions by injecting the attention mechanism into the CNN-backbones.

Overall, the attention mechanism of Transformer explicitly interprets each image as a sequence of patches and then integrates objective information across these patches. Different from modeling interactions across patches, DoT captures the sample correspondence and achieves local semantic consistency across domains by proposing a domain-level attention. Additionally, DoT can be connected with OT and statistical learning theory, which provides a new perspective to understanding Transformers for UDA problem.

### 3 METHODOLOGY

For UDA problems, assume that we have access to a labeled source domain  $\mathcal{D}^s = \{(\mathbf{x}_i^s, y_i^s)\}_{i=1}^{n_s}$  and an unlabeled target domain  $\mathcal{D}^t = \{\mathbf{x}_j^t\}_{j=1}^{n_t}$ , where  $\mathbf{x}_i^s, \mathbf{x}_j^t$  represent samples and  $y_i^s \in \{1, 2, \dots, K\}$  denotes the ground-truth label of  $\mathbf{x}_i^s$ .

We introduce the Domain-Transformer (DoT) for UDA problem in Section 3.1, which can be a plug-and-play module for many deep network-based models. Then, the mathematical connection between DoT and OT algorithm is presented in Section 3.2. The generalization error bound is derived from the perspective of learning theory in Section 3.3. These results provide insights into understanding the inherency of DoT. Finally, the local structure regularization for discriminability and the overall algorithm are presented in Section 3.4 and Section 3.5, respectively.

#### 3.1 Domain-Transformer

We first propose the DoT method with the cross-attention mechanism, which is helpful to build the classification-oriented sample correspondence across domains.

Different from the explicit position information of sentences in NLP, samples from the two domains are position-free. We can explore the implicit locality structures across domains in a semantic latent space. Since CNNs have achieved remarkable success in visual tasks, we still use CNN-backbones as the feature extractor  $G(\cdot)$ . Then, the feature vectors of the source and target domains are represented by

$$\mathbf{G}^s = G(\mathbf{X}^s) \quad \text{and} \quad \mathbf{G}^t = G(\mathbf{X}^t), \quad (1)$$

respectively, where  $\mathbf{G}^s \in \mathbb{R}^{n_s \times d_1}$  and  $\mathbf{G}^t \in \mathbb{R}^{n_t \times d_1}$ .

In this paper, we interpret the long-range dependency between samples across domains by proposing the domain-level attention, in which the *queries* come from the source domain and the *key-value pairs* are derived from the target domain. To keep consistency with the Transformer, we use the fully-connected networks (FCNs) to simulate the separate and learnable projections of queries and key-value pairs. These two FCNs for the source domain and the target domain are denoted as  $F_s(\cdot)$  and  $F_t(\cdot)$ , respectively, which can be embedded into the whole network architecture and then trained in an end-to-end manner. The *queries* and *keys* (*values*) can be formulated by

$$\mathbf{F}^s = F_s(\mathbf{G}^s), \quad \mathbf{F}^t = F_t(\mathbf{G}^t), \quad (2)$$

where  $\mathbf{F}^s = [\mathbf{f}_1^s, \mathbf{f}_2^s, \dots, \mathbf{f}_{n_s}^s]^T \in \mathbb{R}^{n_s \times d_2}$  and  $\mathbf{F}^t \in \mathbb{R}^{n_t \times d_2}$ .

As shown in the middle of Figure 2, DoT exchanges semantic information of samples across domains. This procedure is achieved by the domain-level attention mechanism, which formulates the attention map  $\mathbf{A} \in \mathbb{R}^{n_s \times n_t}$



(also known as attention score matrix) as the expression coefficients across domains, i.e.,

$$\mathbf{A} = \text{softmax} \left( \frac{\mathbf{F}^s \mathbf{F}^t T}{\sqrt{d_2}} \right), \quad (3)$$

or

$$a_{ij} = \frac{\exp(\mathbf{f}_i^{sT} \mathbf{f}_j^t / \sqrt{d_2})}{\sum_{i=1}^{n_t} \exp(\mathbf{f}_i^{sT} \mathbf{f}_j^t / \sqrt{d_2})}. \quad (4)$$

The softmax function is applied to the rows of the scaled similarity matrix  $\frac{\mathbf{F}^s \mathbf{F}^t T}{\sqrt{d_2}}$ , which characterizes the pair-wise similarities between the source feature  $\mathbf{X}^s$  and the target sample  $\mathbf{X}^t$  in the feature subspace. Specifically, the  $i$ -th row of  $\mathbf{A}$  represents the similarities between *query*  $\mathbf{f}_i^s$  and all *keys*  $\{\mathbf{f}_j^t\}_{j=1}^{n_t}$ . Thus, it can be viewed as a competitive expression of sample correspondence intensity. If the attention weight  $a_{ij}$  is larger, the source feature  $\mathbf{f}_i^s$  will allocate more attention to the target feature  $\mathbf{f}_j^t$ . The output representations of the domain-transformer module, i.e., the transformed source features (also called transformed *queries*)  $\hat{\mathbf{F}}^s$ , can be represented by

$$\hat{\mathbf{F}}^s = \mathbf{A} \mathbf{F}^t \in \mathbb{R}^{n_s \times d_2}. \quad (5)$$

For each *query*  $\mathbf{f}_i^s$ , it can be observed that the transformed *query*  $\hat{\mathbf{f}}_i^s$  is a weighted sum of *keys*  $\{\mathbf{f}_j^t\}_{j=1}^{n_t}$ . Among all the feature vectors  $\{\mathbf{f}_j^t\}_{j=1}^{n_t}$  in the target domain, those more similar to *query*  $\mathbf{f}_i^s$  in the source domain will have a larger attention weight  $a_{ij}$ , and they contribute more to the transformed *query*  $\hat{\mathbf{f}}_i^s$ . Though there is a discrepancy between source and target domains, feature vectors in the same class but different domains are expected to be more similar. Thus, each transformed *query*  $\hat{\mathbf{f}}_i^s$  is mainly weighted by the most relevant *values/keys* in  $\{\mathbf{f}_j^t\}_{j=1}^{n_t}$ . In this perspective, the attention map  $\mathbf{A}$  characterizes long-range dependency and capture the correspondence between samples in the same class but different domains. Thus, the transformed *queries*  $\hat{\mathbf{F}}^s$  can be considered as the image of the source features  $\mathbf{F}^s$  in the subspace of the target domain. Since  $\hat{\mathbf{F}}^s$  retains labels of  $\mathbf{F}^s$ , the classifier  $C(\cdot)$  trained on  $\hat{\mathbf{F}}^s$  is expected to be generalized well to the target domain.

### 3.2 Connection between DoT and OT

Both the similarity estimation approach and the transformation manner, as shown in Eq. (4) and Eq. (5), encourage us to explore further intrinsic connection between DoT and the OT algorithm. The relationship will provide an insight into understanding the inherency of Transformers. Moreover, it implies that the domain discrepancy can be explicitly mitigated in DoT model. This is just very important to deal with the UDA problem effectively.

In the context of domain adaptation, once the attention map  $\mathbf{A}$  has been computed, the sample correspondence between the source and the target domains can be considered as determined. It is interesting that the attention map  $\mathbf{A}$  shown in Eq. (3) has an intrinsic connection with the optimal transport/assignment plan. Here we denote

$\Omega = \{\gamma \in \mathbb{R}_+^{n_s \times n_t} \mid \gamma \mathbf{1}_{n_t} = \mu_s, \gamma^T \mathbf{1}_{n_s} = \mu_t\}$ . The entropy-regularized Kantorovich formulation of the OT problem [43] is defined as

$$\arg \min_{\gamma \in \Omega} \langle \gamma, \mathbf{M} \rangle_F + \lambda H(\gamma), \quad (6)$$

where  $\langle \cdot, \cdot \rangle_F$  is the Frobenius dot product,  $\mathbf{M}$  is the cost matrix, and  $H(\gamma) = \sum_{i,j} \gamma_{ij} \log \gamma_{ij}$ . Generally, the squared  $\ell_2$  distance, i.e.,  $M_{ij} = \|\mathbf{f}_i^s - \mathbf{f}_j^t\|_2^2$ , is used to compute the cost matrix. For  $\lambda > 0$ , the OT solution  $\gamma^*$  of Eq. (6) is unique and has the form [43]

$$\gamma^* = \text{diag}(\mu) \exp \left( -\frac{\mathbf{M}}{\lambda} \right) \text{diag}(\nu), \quad (7)$$

where  $\mu \in \mathbb{R}^{n_s}$  and  $\nu \in \mathbb{R}^{n_t}$  are two none-negative vectors. It can be recast into a bi-stochastic matrix scaling problem [44] and then solved by the Sinkhorn-Knopp Algorithm [45]. We can rewrite Eq. (7) as

$$\begin{aligned} \gamma_{ij}^* &= \mu_i \exp(-M_{ij}/\lambda) \nu_j \\ &= \mu_i \exp(-\|\mathbf{f}_i^s - \mathbf{f}_j^t\|_2^2 / \lambda) \nu_j \\ &\propto \mu_i \exp(2(\mathbf{f}_i^s)^T \mathbf{f}_j^t / \lambda) \nu_j. \end{aligned} \quad (8)$$

Compared Eq. (8) with Eq. (4), it can be observed that both  $a_{ij}$  of the attention map and  $\gamma_{ij}^*$  of the OT plan are based on the matrix scaling problem of  $\exp(\mathbf{f}_i^{sT} \mathbf{f}_j^t)$ . More specifically, by setting  $\lambda = 2\sqrt{d_2}$ , it is row-stochastic for the attention map  $\mathbf{A}$ , while doubly-stochastic for the OT plan due to its double constraints on marginal distributions. Thus,  $\gamma^*$  is empirically much sparser than  $\mathbf{A}$ . Intrinsically, columns of  $\hat{\mathbf{F}}^s$  are sparsely linear combination of those in  $\mathbf{F}^t$ . In this perspective, the attention map  $\mathbf{A}$  has some equivalence to barycentric mapping induced by the optimal transport plan  $\gamma$ . Therefore, some appealing properties of the optimal transport literature can be explored in our DoT method. Suppose that the marginal distribution (w.r.t. features) of the source domain and the target domain is  $\mu_s$  and  $\mu_t$ , respectively. We can interpolate the two distributions by the geodesics of the Wasserstein metric [46], parameterized by a scalar  $t \in [0, 1]$ . This defines a new or intermediate distribution  $\hat{\mu}$  such that

$$\hat{\mu} = \arg \min_{\mu} t \mathcal{W}_2^2(\mu_s, \mu) + (1-t) \mathcal{W}_2^2(\mu_t, \mu).$$

This distribution boils down to [46]

$$\hat{\mu} = \sum_{i,j} \gamma_{ij} \delta_{(1-t)\mathbf{f}_i^s + t\mathbf{f}_j^t}.$$

As a result, we can map samples in the source domain onto the target domain by selecting  $t = 0$ . Then, the intermediate distribution  $\hat{\mu}$  is a distribution with the same support of  $\mu_t$ , and we have  $\hat{\mu} = \sum_j \hat{p}_j^t \delta_{\mathbf{f}_j^t}$ , with  $\hat{p}_j^t = \sum_i \gamma_{ij}$ . Note the weights  $\hat{p}_j^t$  is the sum of weights between all source samples  $\mathbf{f}_i^s$  and the target sample  $\mathbf{f}_j^t$ . Recall that  $a_{ij}$  tells us how much probability mass of  $\mathbf{f}_i^s$  is transferred to  $\mathbf{f}_j^t$ , by comparing the attention matrix with the optimal transport plan. Along this line, we can exploit the domain-level attention as the following barycentric mapping based on the equivalence in Eq. (8), i.e.,

$$\hat{\mathbf{f}}_i^s = \arg \min_{\mathbf{z} \in \mathbb{R}^{d_2}} \sum_j \gamma_{ij} m(\mathbf{z}, \mathbf{f}_j^t),$$

where  $m$  denotes the distance metric,  $\mathbf{f}_j^t$  is a given feature vector in the target domain and  $\hat{\mathbf{f}}_i^s$  is its transformed representation. In particular, when the distance function is the squared  $\ell_2$  metric, this barycenter corresponds to a weighed average and the sample is mapped into the convex hull of the target samples [2]. For all samples in the source domain, the barycentric mapping has an analytic formulation as

$$\hat{\mathbf{F}}^s = \mathbf{T}_\gamma(\mathbf{F}^s) = \text{diag}(\gamma \mathbf{1}_{n_t})^{-1} \gamma \mathbf{F}^t = \mathbf{A} \mathbf{F}^t, \quad (9)$$

where  $\mathbf{1}_{n_t}$  is the all-ones vector in  $\mathbb{R}^{n_t}$ , and  $\mathbf{T}_\gamma$  denotes the optimal transport map associating with the transport plan  $\gamma$ . This result has multiple important meanings in domain adaptation. It is a first-order approximation of the true  $n_s$  Wasserstein barycenters of the target distribution, as stated by Courty *et al.* [2]. Moreover, the projection matrix  $\text{diag}(\gamma \mathbf{1}_{n_t})^{-1} \gamma$  is the (row)-normalized similarity weights in the attention mechanism, as shown in Eq. (5). Therefore, it builds an intrinsic connection between DoT and the optimal transportation, and thus presents a reasonable interpretation for the effectiveness of our DoT method.

### 3.3 Theoretical Analysis

Based on the connection between DoT and OT algorithms, an informative generalization bound for UDA can be derived from the perspective of learning theory. The theoretical results provide the insights into understanding the proposed domain-attention mechanism in UDA problem.

To theoretically analyze the generalization performance of DoT method, a generalization bound with the Wasserstein metric-based discrepancy is necessary. We consider the domain adaptation problem in the bi-class setting, with continuous outputs, as follows. To facilitate the characterization of distribution gap and labeling discrepancy, we define a domain as a pair consisting of a distribution  $P_X$  on input  $\mathcal{X}$  and a labeling function  $f : \mathcal{X} \rightarrow [0, 1]$ , which can have a fractional (expected) value when labeling occurs non-determinedly. More specifically, we denote by  $(P_X^s, f_s)$  the source domain and  $(P_X^t, f_t)$  the target domain. A hypothesis space  $\mathcal{H}$  is a set of hypotheses  $h : \mathcal{X} \rightarrow [0, 1]$ .

**Definition 1 (True Risk)** The true risk is defined as the probability according to the distribution  $P_X^s$  that a hypothesis  $h$  disagrees with a labeling function  $f_s$  (which can also be a hypothesis), i.e.,

$$\epsilon_s(h, f_s) := \mathbb{E}_{x \sim P_X^s} [|h(x) - f_s(x)|].$$

Note that the true risk satisfies the triangle inequality, i.e.,  $\epsilon_s(h_1, h_3) \leq \epsilon_s(h_1, h_2) + \epsilon_s(h_2, h_3)$ , for any hypotheses  $h_1, h_2$  and  $h_3 \in \mathcal{H}$ . When we want to refer to the source error of a hypothesis, we use the shorthand  $\epsilon_s(h) = \epsilon_s(h, f_s)$ . Without loss of generality, we use the parallel notations  $\epsilon_t(h, f_t)$  and  $\epsilon_t(h)$  for the target domain.

Then we introduce some preliminary definitions on the probability metric, which will be used to reformulate the risk function as the (domain) distribution discrepancy.

**Definition 2 (Seminorm)** Let  $\mathcal{F}$  be a function space. A real valued function  $\rho : \mathcal{F} \rightarrow \mathbb{R}$  is called a seminorm if it satisfies the following two conditions.

- *Subadditivity inequality:*  $\rho(f_1 + f_2) \leq \rho(f_1) + \rho(f_2)$  for any  $f_1, f_2 \in \mathcal{F}$ ;

- *Absolute homogeneity:*  $\rho(af) = |a|\rho(f)$  for any  $f \in \mathcal{F}$  and all scalars  $a$ .

Note that these two conditions imply that  $\rho(0) = 0$  and that every seminorm  $\rho$  also has the *Nonnegativity* property:  $\rho(f) \geq 0$  for any  $f \in \mathcal{F}$ .

**Definition 3 (Sobolev Seminorm)** Let  $(\mathcal{X}, d)$  be a metric space. For any real valued function  $f$  on  $\mathcal{X}$ , its Sobolev seminorm is defined as

$$\|f\|_{H^1} := \left( \int \|\nabla f(x)\|^2 dx \right)^{\frac{1}{2}}.$$

**Definition 4 (Integral Probability Metric (IPM))** Let  $\mathcal{F}$  be a class of real-valued bounded measurable functions on  $\mathcal{X}$ . The IPM between two distributions  $P_X^s$  and  $P_X^t$  is defined as

$$d(P_X^s, P_X^t) := \sup_{f \in \mathcal{F}} \left| \mathbb{E}_{x \sim P_X^s} [f(x)] - \mathbb{E}_{x \sim P_X^t} [f(x)] \right|. \quad (10)$$

Choosing  $\mathcal{F} = \{f : \|f\|_{H^1} \leq 1\}$  in Eq. (10) yields

$$\|P_X^s - P_X^t\|_{H^{-1}} := \sup_{f : \|f\|_{H^1} \leq 1} \left| \mathbb{E}_{x \sim P_X^s} [f(x)] - \mathbb{E}_{x \sim P_X^t} [f(x)] \right|.$$

Furthermore, there exists two positive constants  $c_1$  and  $c_2$  such that [47], [48]

$$c_1 \|P_X^s - P_X^t\|_{H^{-1}} \leq \mathcal{W}_2(P_X^s, P_X^t) \leq c_2 \|P_X^s - P_X^t\|_{H^{-1}}.$$

It indicates that  $H^{-1}$  norm, which is the dual norm of the Sobolev seminorm, is equivalent to the 2-Wasserstein  $\mathcal{W}_2$  distance. In other words, the  $\mathcal{W}_2$  distance gives an upper bound on an integral probability metric in  $\mathcal{F}$ .

**Remark** This equivalence implies that the disagreement of any hypothesis on two feature distributions is upper-bounded by the 2-Wasserstein distance between them. Thus, the inequality can be employed to reformulate the hypotheses' distance in risk objective as  $\mathcal{W}_2$  between feature distributions, which is actually the discrepancy between transformed features in Eq. (5).

Next we will show the generalization error bounded by  $\mathcal{W}_2$  distance across domains. Generally, we assume the hypothesis space  $\mathcal{H} = \mathcal{F}$ , which is reasonable for regression task or binary classification with probability output. First, we bound the distance between the true risks across domains as the following lemma.

**Lemma 1** For any hypotheses  $h_1, h_2 \in \mathcal{H}$ , there exists a positive constant  $c$  such that

$$|\epsilon_s(h_1, h_2) - \epsilon_t(h_1, h_2)| \leq c \mathcal{W}_2(P_X^s, P_X^t).$$

**Proof** For any  $h_1, h_2 \in \mathcal{H}$ , denote  $\bar{h} = \frac{h_1 - h_2}{2}$ . Note that  $\bar{h}$  still belongs to  $\mathcal{H}$  since

$$\|\bar{h}\|_{H^1} = \left\| \frac{h_1 - h_2}{2} \right\|_{H^1} \leq \frac{\|h_1\|_{H^1} + \|h_2\|_{H^1}}{2} \leq 1.$$

Now we prove the main inequality.

$$\begin{aligned}
& |\epsilon_s(h_1, h_2) - \epsilon_t(h_1, h_2)| \\
&= 2 \left| \mathbb{E}_{x \sim P_X^s} \left[ \frac{h_1(x) - h_2(x)}{2} \right] - \mathbb{E}_{x \sim P_X^t} \left[ \frac{h_1(x) - h_2(x)}{2} \right] \right| \\
&= 2 \left| \mathbb{E}_{x \sim P_X^s} [\bar{h}(x)] - \mathbb{E}_{x \sim P_X^t} [\bar{h}(x)] \right| \\
&\leq 2 \sup_{h \in \mathcal{H}} \left| \mathbb{E}_{x \sim P_X^s} [h(x)] - \mathbb{E}_{x \sim P_X^t} [h(x)] \right| \\
&= 2 \|P_X^s - P_X^t\|_{H^{-1}} \\
&\leq c\mathcal{W}_2(P_X^s, P_X^t).
\end{aligned}$$

Based on this lemma, we now connect the generalization error with the  $\mathcal{W}_2$  distance (similar to [6, Theorem 2]). Note that the above lemma cannot be directly applied to labeling function  $f_s$  and  $f_t$ , since they may not be a hypothesis. Usually, to ensure the tightness of upper bound, we define an intermediate hypothesis  $h^*$  which minimizes the joint error as

$$h^* = \arg \inf_{h \in \mathcal{H}} \epsilon_s(h) + \epsilon_t(h).$$

We denote the optimal joint error of the intermediate hypothesis  $h^*$  as  $\lambda = \epsilon_s(h^*) + \epsilon_t(h^*)$ .

**Theorem 1** Assuming  $\mathcal{H}$  is a hypothesis space satisfies that  $\|h\|_{H^1} \leq 1$  for any  $h \in \mathcal{H}$ . Let  $P_X^s$  and  $P_X^t$  be the marginals over  $\mathcal{X}$  of the source and target domains, respectively. Then for any  $h \in \mathcal{H}$ , there exists a positive constant  $c$  such that

$$\epsilon_t(h) \leq \epsilon_s(h) + c\mathcal{W}_2(P_X^s, P_X^t) + \lambda.$$

**Proof**

$$\begin{aligned}
\epsilon_t(h) &= \epsilon_t(h, f_t) \\
&\leq \epsilon_t(h, h^*) + \epsilon_t(h^*, f_t) \\
&\leq \epsilon_s(h, h^*) + c\mathcal{W}_2(P_X^s, P_X^t) + \epsilon_t(h^*, f_t) \\
&\leq \epsilon_s(h, f_s) + \epsilon_s(h^*, f_s) + c\mathcal{W}_2(P_X^s, P_X^t) + \epsilon_t(h^*, f_t) \\
&= \epsilon_s(h) + c\mathcal{W}_2(P_X^s, P_X^t) + \lambda.
\end{aligned}$$

Theorem 1 shows that the generalization is bounded by the  $\mathcal{W}_2$  distance across domains. Note that  $\mathcal{W}_2$  is generally smaller than the  $\mathcal{H}\Delta\mathcal{H}$  divergence in [6, Theorem 2] where the  $\mathcal{H}$  can be any function space. Thus, the generalization bound in Theorem 1 with  $\mathcal{W}_2$  distance is generally tighter. Further, if the labeling functions  $f_s$  and  $f_t$  belong to the hypothesis space  $\mathcal{H}$ , we can deduce a more informative upper bound without the intractable constant  $\lambda$ .

**Theorem 2** Assuming  $\mathcal{H}$  is a hypothesis space satisfies that  $\|h\|_{H^1} \leq 1$  for any  $h \in \mathcal{H}$ , and  $f_s, f_t \in \mathcal{H}$ . Let  $P_X^s$  and  $P_X^t$  be the marginals over  $\mathcal{X}$  of the source and target domains, respectively. Then for any  $h \in \mathcal{H}$ , there exists a positive constant  $c$  such that

$$\epsilon_t(h) \leq \epsilon_s(h) + c\mathcal{W}_2(P_X^s, P_X^t) + \min \{\epsilon_s(f_s, f_t), \epsilon_t(f_s, f_t)\}.$$

**Proof** If we apply the Lemma 1 first, then

$$\begin{aligned}
\epsilon_t(h) &= \epsilon_t(h, f_t) \\
&\leq \epsilon_s(h, f_t) + c\mathcal{W}_2(P_X^s, P_X^t) \\
&\leq \epsilon_s(h, f_s) + c\mathcal{W}_2(P_X^s, P_X^t) + \epsilon_s(f_s, f_t).
\end{aligned}$$

If we apply triangle inequality of true risk first, then

$$\begin{aligned}
\epsilon_t(h) &= \epsilon_t(h, f_t) \\
&\leq \epsilon_t(h, f_s) + \epsilon_t(f_s, f_t) \\
&\leq \epsilon_s(h, f_s) + c\mathcal{W}_2(P_X^s, P_X^t) + \epsilon_t(f_s, f_t).
\end{aligned}$$

By combining the inequality above, we have

$$\epsilon_t(h) \leq \epsilon_s(h) + c\mathcal{W}_2(P_X^s, P_X^t) + \min \{\epsilon_s(f_s, f_t), \epsilon_t(f_s, f_t)\}.$$

**Remark** Under the covariate shift assumption, the labeling functions of different domains are the same, i.e.,  $f = f_s = f_t$ . Then the bound of Theorem 2 boils down to

$$|\epsilon_s(h) - \epsilon_t(h)| \leq c\mathcal{W}_2(P_X^s, P_X^t).$$

It implies that minimizing the Wasserstein distance across domains is sufficient for successful domain adaptation.

Note that the domain-level transformer in DoT is mathematically analogous to the barycentric mapping in OT. Then, the generalization upper-bounds in Theorem 1-2 implies that the true risk on target domain can be bounded by the DoT model. These results ensure that the domain-level transformer module can explicitly reduce the domain discrepancy and enhance the model's transferability with the OT-like mapping Eq. (9).

Further we consider the upper bound with empirical estimator. Denote  $\mathbf{X}^s$  and  $\mathbf{X}^t$  be the samples drawn according  $P_X^s$  and  $P_X^t$  with sample size  $n$ , respectively. Then the empirical distributions of  $\mathbf{X}^s$  and  $\mathbf{X}^t$  is denoted as  $\hat{P}_X^s$  and  $\hat{P}_X^t$ , respectively.

**Theorem 3 (Rate of Wasserstein Distance)** [48] Let  $\mathcal{X} = \mathbb{R}^d$  and measures  $(P_X^s, P_X^t)$  are supported on bounded domain. For any  $d > 2$  and  $1 \leq p < +\infty$ ,

$$\begin{aligned}
& \mathbb{E}_{(\hat{P}_X^s, \hat{P}_X^t) \sim (P_X^s, P_X^t)^n} \left[ |\mathcal{W}_p(\hat{P}_X^s, \hat{P}_X^t) - \mathcal{W}_p(P_X^s, P_X^t)| \right] \\
& \lesssim \mathcal{O}(n^{-\frac{1}{d}}).
\end{aligned}$$

The notation  $f_1(n) \lesssim f_2(n)$  indicates that there exists a constant  $\tilde{c}$ , depending on  $f_1$  and  $f_2$  but not  $n$ , such that  $f_1(n) \leq \tilde{c}f_2(n)$ . Theorem 3 implies that the empirical Wasserstein distance  $\mathcal{W}_p(\hat{P}_X^s, \hat{P}_X^t)$  is asymptotically consistent. Based on this asymptotic property of Wasserstein distance, we could prove the generalization upper bound with empirical Wasserstein distance.

**Corollary 1 (Empirical Generalization Upper Bound)**

Assuming  $\mathcal{H}$  is a hypothesis space satisfies that  $\|h\|_{H^1} \leq 1$  for any  $h \in \mathcal{H}$ . Let  $P_X^s$  and  $P_X^t$  be the marginals over  $\mathcal{X} = \mathbb{R}^d$  of the source and target domains, respectively. Denote  $\hat{P}_X^s$  and  $\hat{P}_X^t$  as the empirical distributions of samples drawn according to  $P_X^s$  and  $P_X^t$  with sample size  $n$ , respectively. Then for any  $h \in \mathcal{H}$ , there exists a positive constant  $c$  such that the following holds with high probability:

$$\epsilon_t(h) \leq \epsilon_s(h) + 2c\mathcal{W}_2(\hat{P}_X^s, \hat{P}_X^t) + \lambda + \mathcal{O}(n^{-\frac{1}{d}}).$$

Furthermore, if  $f_s, f_t \in \mathcal{H}$ , then the following holds with high probability:

$$\begin{aligned}
\epsilon_t(h) &\leq \epsilon_s(h) + 2c\mathcal{W}_2(\hat{P}_X^s, \hat{P}_X^t) \\
&\quad + \min \{\epsilon_s(f_s, f_t), \epsilon_t(f_s, f_t)\} + \mathcal{O}(n^{-\frac{1}{d}}).
\end{aligned}$$

Corollary 1 implies that the empirical generalization upper bound will converge to the truth with the increasing sample size. It ensures that the risk with finite samples is still bounded by the DoT model while the appealing property of DoT is also valid in empirical case.

### 3.4 Local Structure Regularization

Though the transferability of DoT model was analyzed in previous sections, it is also necessary to enhance discriminability of the model. In this section, we explore the locality regularization terms for local semantic consistency learning, which are usually formulated by manifolds or graphs. This procedure will promote a group-sparse or class-sparse attention matrix in essence.

Generally, the domain-level attention encodes the relevant target feature vectors for each source feature vector. It is desirable that similar samples in the source domain also be similar after application of the domain-level attention. Since larger weights indicate higher similarities, those relevant target feature vectors are expected to share the same class label with the corresponding source feature vector. This is especially important in transferring discriminant features across different domains.

#### 3.4.1 Unsupervised Local Structure Learning

The Locality Preserving Projection (LPP) algorithm [49] can be explored to incorporate neighborhood information in the target domain. Firstly, we construct the adjacency graph via  $k$  nearest neighbors with the Euclidean distance. Each pair of nodes is connected once one node is among  $k$  nearest neighbours of the other node. Then, the adjacency matrix  $\mathbf{W}^t$  is defined by a binary variable, i.e.,  $w_{ij}^t = 1$  if and only if the vertices  $i$  and  $j$  are connected by an edge, and  $w_{ij}^t = 0$  otherwise. The objective of unsupervised local structure learning for the target domain is formulated as

$$\mathcal{L}_t(\theta_G, \theta_{F_t}) = \sum_{i,j}^{n_t} \|\mathbf{f}_i^t - \mathbf{f}_j^t\|_2^2 w_{ij}^t. \quad (11)$$

The entropy criterion is also utilized to explore intrinsic locality structure of the target domain. Mathematically, the entropy loss  $\mathcal{L}_{ent}$  is formulated as

$$\mathcal{L}_{ent}(\theta_G, \theta_{F_t}, \theta_C) = \frac{1}{n_t} \sum_{j=1}^{n_t} \sum_{k=1}^K -\hat{p}_{jk}^t \log \hat{p}_{jk}^t, \quad (12)$$

where  $\hat{p}_{jk}^t = C(F_t(G(\mathbf{x}_j^t)))$  satisfying to  $\sum_{k=1}^K \hat{p}_{jk}^t = 1$  is the prediction probability of  $\mathbf{x}_j^t$  belonging to the  $k$ -th class.

#### 3.4.2 Supervised Local Structure Preserving

The labels of  $\hat{\mathbf{F}}^s$  are the same with those of  $\mathbf{F}^s$ . In order to preserve discriminative structure of the source domain, we still use LPP on the transformed source domain and formulate the regularization term as

$$\mathcal{L}_s(\theta_G, \theta_{F_s}, \theta_{F_t}) = \sum_{i,j}^{n_s} \|\hat{\mathbf{f}}_i^s - \hat{\mathbf{f}}_j^s\|_2^2 w_{ij}^s, \quad (13)$$

where

$$w_{ij}^s = \begin{cases} 1, & \text{if } y_i^s = y_j^s, \\ 0, & \text{else.} \end{cases}$$

### Algorithm 1 DoT for unsupervised domain adaptation

---

**Input:**  $\mathcal{D}^s = \{\mathbf{x}_i^s, y_i^s\}_{i=1}^{n_s}$ ,  $\mathcal{D}^t = \{\mathbf{x}_j^t\}_{j=1}^{n_t}$ , batch-sizes  $b_s, b_t$ .  
**Output:** Networks parameters  $\theta$ , predictions  $\{\hat{y}_j^t\}_{j=1}^{n_t}$ .

- 1: Make random mini-batch divisions of  $\mathcal{D}^s$  and  $\mathcal{D}^t$ .  
 %% Training Stage
- 2: **for** each batch  $\mathcal{B}^s = \{\mathbf{x}_i^s, y_i^s\}_{i=1}^{b_s}$  **do**
- 3:   Pre-train  $G(\cdot)$ ,  $F_s(\cdot)$  and  $C(\cdot)$  via Eq. (14);
- 4: **end for**
- 5: Initialize  $F_t(\cdot)$  by the pre-trained  $F_s(\cdot)$ .
- 6: **while** not converged **do**
- 7:   **for** batch  $\mathcal{B}^s = \{\mathbf{x}_i^s, y_i^s\}_{i=1}^{b_s}$  and  $\mathcal{B}^t = \{\mathbf{x}_j^t\}_{j=1}^{b_t}$  **do**
- 8:     Obtain deep features  $\mathbf{G}^s$  and  $\mathbf{G}^t$  from Eq. (1);  
 % Domain-level attention
- 9:     Project  $\mathbf{G}^s$  and  $\mathbf{G}^t$  into queries  $\mathbf{F}^s$  and keys/values  $\mathbf{F}^t$ , with different projections, via Eq. (2);
- 10:     Get the attention matrix  $\mathbf{A}$  via Eq. (3), and then obtain the transformed source features  $\hat{\mathbf{F}}^s$  via Eq. (5);  
 % Preparation of Local Structure Learning
- 11:     Get the local regularization terms  $\mathcal{L}_t$  and  $\mathcal{L}_s$  via Eq. (11) and Eq. (13);
- 12:     Get the entropy loss  $\mathcal{L}_{ent}$  via Eq. (12);  
 % Update the overall objective
- 13:     Update  $\theta$  by minimizing Eq. (15);
- 14:   **end for**
- 15: **end while**  
 %% Test Stage
- 16: **for** each batch  $\mathcal{B}^t = \{\mathbf{x}_j^t\}_{j=1}^{b_t}$  **do**
- 17:   Forward propagate  $\mathcal{B}^t$  to obtain  $\mathbf{F}^t$ , and then predict the probability  $\hat{\mathbf{p}}^t$  by  $C(\cdot)$ ;
- 18:   Compute predictions as  $\hat{y}_j^t = \arg \max_k \hat{p}_{jk}^t$ ;
- 19: **end for**
- 20: **return** Networks parameters  $\theta$ , predictions  $\{\hat{y}_j^t\}_{j=1}^{n_t}$ .

---

By minimizing the discriminant regularization term in Eq. (13), samples from the same class are expected to be projected close to each other in the subspace.

### 3.5 Algorithm and Optimization

DoT transforms the source feature vectors into target domain via the domain-level attention, and then it learns discriminative features with the help of local structure regularization. As shown in Eq. (9), the transformed source feature vectors  $\hat{\mathbf{F}}^s$  and the target feature vectors  $\mathbf{F}^t$  are in the shared subspace, the classifier trained on  $\hat{\mathbf{F}}^s$  can be hopefully transferred to the target domain with a small generalization error. It implies that the domain alignment is implicitly achieved by DoT without introducing the explicit domain discrepancy optimization. Then, the empirical risk of model can be directly estimated on the transformed source domain, i.e.,

$$\mathcal{L}_{tce}(\theta) = \frac{1}{n_s} \sum_{i=1}^{n_s} l_{ce}(C(\hat{\mathbf{f}}_i^s), y_i^s; \theta_G, \theta_{F_t}, \theta_C), \quad (14)$$

where  $l_{ce}(\cdot, \cdot)$  is the cross-entropy function, and  $\theta$  represents all the parameters updated in the adaptive feature learning process. Here we use the subscript “tce” to stress that this



loss term is computed by using the transformed source features  $\hat{F}^s$ , rather than  $F^s$ .

The overall objective function of DoT consists of four terms, and it is written as

$$\mathcal{L}(\theta) = \mathcal{L}_{tce}(\theta) + \lambda_1 \mathcal{L}_{ent}(\theta_G, \theta_{F_t}, \theta_C) + \lambda_2 \mathcal{L}_t(\theta_G, \theta_{F_t}) + \lambda_3 \mathcal{L}_s(\theta_G, \theta_{F_s}, \theta_{F_t}), \quad (15)$$

where  $\lambda_1, \lambda_2$  and  $\lambda_3 > 0$  are trade-off hyper-parameters. The locality preserving term  $\mathcal{L}_s$  is built upon the domain-level attention mechanism to preserve discriminative structure in the source domain. The locality preserving term  $\mathcal{L}_t$  and the entropy  $\mathcal{L}_{ent}$  are used to explore intrinsic structure in the target domain, and then keep similar samples nearby in the latent subspace. Thus, each row of the attention matrix will have group-sparsity, and more relevant target feature vectors will make larger contribution to the corresponding outputs of the domain-transformer module.

The main optimization procedure has been summarized in Algorithm 1. The domain-level transformer projects the source domain into the target domain, thus, it is expected that the discriminant structure can be learned and transferred from the source domain to the target domain, either. Enhanced by the local semantic consistency learning phase, samples within the same underlying class but different domains will be drawn closer. Finally, the classifier  $C(\cdot)$  is learned from the transformed source domain, and it is expected to fit the target domain well.

## 4 EXPERIMENTS

In this section, DoT is evaluated and compared with several state-of-the-art methods. In Section 4.1, we introduce the datasets and experimental setting. In Section 4.2, we show the experimental results on four benchmark datasets, and then present ablation study and further analysis, including parameter sensitivity and feature visualization.

### 4.1 Datasets and Experimental Setting

The datasets are briefly introduced as follows.

**ImageCLEF-DA** [53] consists of 3 domains from 12 classes. The domains include *Caltech* (C), *ImageNet* (I) and *Pascal* (P). It is a domain-balanced dataset as each domain has 600 images and each class has the same size.

**Office-31** [54] consists of 3 domains, with 4,652 images from 31 classes of office objects. The domains include *Amazon* (A) (images downloaded from online merchants), *Webcam* (W) (low-resolution images from a web camera) and *DSLR* (D) (high-resolution images from a digital SLR camera). This dataset not only captures a large intra-class variation, but also represents several different visual domain shifts.

**Office-Home** [55] consists of 4 domains, with around 15,500 images from 65 classes of everyday objects. There is an average of around 70 images in each class and 99 images at most. The domains include *Art* (Ar), *Clipart* (Cl), *Product* (Pr) and *Real-World* (Rw).

**VisDA-2017** [56] is a challenging large-scale dataset with over 280K images in 12 classes. It aims to transfer knowledge from the source domain *synthetic* (S) to the target domain *real-image* (R). S includes 152,397 synthetic images

generated by 3D models and R collects 55,388 object images from the Microsoft COCO database [57]. Task  $S \rightarrow R$  will be used to algorithm evaluation.

In the following experiments, we adopt the ResNet [25] pre-trained on ImageNet [58] as feature extractor  $G(\cdot)$  in DoT. Specifically, ResNet-50 is used for ImageCLEF-DA, Office-31 and Office-Home, while ResNet-101 is used for VisDA-2017. The domain-specific projections  $F_s(\cdot)$  and  $F_t(\cdot)$  use the same architecture, which has three fully-connected layers for VisDA-2017 while two full-connected layers for other datasets. The classifier  $C(\cdot)$  is a single fully-connected layer followed by the softmax activation function. We implement DoT with PyTorch framework and train the network parameters with Gradient Descent (GD) by Adam Optimizer. To learn the transferable features, we fix the pre-trained CNNs while training DoT and classifier with batch GD on Office-31, Office-Home, ImageCLEF-DA and mini-batch GD on VisDA-2017 ( $b_s = b_t = 5,000$ ). For simplicity, the whole model is abbreviated as **DoTNet** in experiments.

### 4.2 Results and Analysis

**Comparison.** We use some state-of-the-art methods for evaluation and comparison. The compared methods can be roughly categorized into three groups. The first group consists of the statistic alignment methods including DAN [3], JAN [18], TPN [35] and CKB [22]. The second group consists of the adversarial domain adaptation methods including DANN [10], CDAN [20], CDAN+E [20] and TADA [39]. The third group consists of the geometric metric and optimal transport-based methods including KGOT [13], DeepJDOT [14], ETD [15], SWD [59] and DMP [5]. SAFN [51], DSAN [34] and ATM [52] are also used for extensive comparison. The results across four benchmark datasets are shown in Tables 1-3, which are expected to validate the effectiveness of DoT in dealing with the UDA problems.

The results of ImageCLEF-DA are shown in the left of Table 1. The mean accuracies of OT-based methods, i.e., KGOT, ETD and DeepJDOT, are 84.1%, 89.7%, and 86.7%, respectively. Compared with KGOT, ETD and DeepJDOT improve the accuracies by considering label information. It indicates that discriminative feature learning in a supervised manner plays an important role in reducing domain discrepancy. Particularly, the mean accuracy of DoTNet is 91.5%, which is 7.4% higher than that of KGOT. It means that our proposed domain-level attention is effective in achieving local semantic consistency. We also see that the mean accuracy of DoTNet is at least 1.5% higher than that of the manifold alignment-based method DMP and the divergence metric alignment-based method ATM. The mean accuracy of both CKB and DSAN achieves 90.2%, which is 1.3% lower than that of DoTNet. Note that target pseudo-labels are employed in CKB and DSAN, and this utilization may bring additional uncertainty to model training and parameter estimation. In contrast, DoTNet learns discriminative features without pseudo-labels. Thus, DoTNet not only outperforms other methods in the sense of average accuracy, but also has significant improvements on most tasks.

The results of Office-31 are shown in the right of Table 1. The adversarial domain adaptation-based method DANN achieves 82.2% accuracy on average. Based on the adversarial learning of DANN, TADA highlights transferable image

TABLE 1  
Accuracies (%) on Image-CLEF and Office-31 (ResNet-50).

Method	ImageCLEF-DA							Office-31						
	I→P	P→I	I→C	C→I	C→P	P→C	Mean	A→W	D→W	W→D	A→D	D→A	W→A	Mean
Source-Only [50]	74.8	83.9	91.5	78.0	65.5	91.2	80.7	68.4	96.7	99.3	68.9	62.5	60.7	76.1
DAN [3]	74.5	82.2	92.8	86.3	69.2	89.8	82.5	80.5	97.1	99.6	78.6	63.6	62.8	80.4
DANN [10]	75.0	86.0	96.2	87.0	74.3	91.5	85.0	82.0	96.9	99.1	79.7	68.2	67.4	82.2
CDAN+E [20]	77.7	90.7	97.7	91.3	74.2	94.3	87.7	94.1	98.6	<b>100.0</b>	92.9	71.0	69.3	87.7
KGOT [13]	76.3	83.3	93.5	87.5	74.8	89.0	84.1	75.3	96.2	98.4	80.3	65.2	63.5	79.8
DeepJDOT [14]	77.5	90.5	95.0	88.3	74.9	94.2	86.7	88.9	98.5	99.6	88.2	72.1	70.1	86.2
ETD [15]	81.0	91.7	97.9	93.3	79.5	95.0	89.7	92.1	<b>100.0</b>	<b>100.0</b>	88.0	71.0	67.8	86.2
CKB [22]	80.7	93.7	97.0	93.5	79.2	97.0	90.2	-	-	-	-	-	-	-
SAFN [51]	78.0	91.7	96.2	91.1	77.0	94.7	88.1	88.8	98.4	99.8	87.7	69.8	69.7	85.7
DSAN [34]	80.2	93.3	97.2	93.8	<b>80.8</b>	95.9	90.2	93.6	98.3	<b>100.0</b>	90.2	73.5	74.8	88.4
TADA [39]	-	-	-	-	-	-	-	94.3	98.7	99.8	91.6	72.9	73.0	88.4
DMP [5]	80.7	92.5	97.2	90.5	77.7	96.2	89.1	93.0	99.0	<b>100.0</b>	91.0	71.4	70.2	87.4
ATM [52]	80.3	92.9	<b>98.6</b>	93.5	77.8	96.7	90.0	80.2	97.9	<b>100.0</b>	77.5	62.1	61.3	70.0
<b>DoTNet</b>	<b>81.4</b>	<b>95.5</b>	<b>97.8</b>	<b>95.3</b>	<b>80.4</b>	<b>98.3</b>	<b>91.5</b>	<b>94.6</b>	<b>98.6</b>	<b>99.8</b>	<b>93.0</b>	<b>75.8</b>	<b>75.0</b>	<b>89.5</b>

TABLE 2  
Accuracies (%) on Office-Home (ResNet-50).

Office-Home	Ar→Cl	Ar→Pr	Ar→Rw	Cl→Ar	Cl→Pr	Cl→Rw	Pr→Ar	Pr→Cl	Pr→Rw	Rw→Ar	Rw→Cl	Rw→Pr	Mean
Source-Only [50]	34.9	50.0	58.0	37.4	41.9	46.2	38.5	31.2	60.4	53.9	41.2	59.9	46.1
DAN [3]	43.6	57.0	67.9	45.8	56.5	60.4	44.0	43.6	67.7	63.1	51.5	74.3	56.3
DANN [10]	45.6	59.3	70.1	47.0	58.5	60.9	46.1	43.7	68.5	63.2	51.8	76.8	57.6
CDAN+E [20]	50.7	70.6	76.0	57.6	70.0	70.0	57.4	50.9	77.3	70.9	56.7	81.6	65.8
KGOT [13]	36.2	59.4	65.0	48.6	56.5	60.2	52.1	37.8	67.1	59.0	41.9	72.0	54.7
DeepJDOT [14]	48.2	69.2	74.5	58.5	69.1	71.1	56.3	46.0	76.5	68.0	52.7	80.9	64.3
ETD [15]	51.3	71.9	<b>85.7</b>	57.6	69.2	73.7	57.8	51.2	79.3	70.2	57.5	82.1	67.3
CKB [22]	<b>54.7</b>	74.4	77.1	63.7	72.2	71.8	64.1	51.7	78.4	73.1	58.0	82.4	68.5
SAFN [51]	52.0	71.7	76.3	64.2	69.9	71.9	63.7	51.4	77.1	70.9	57.1	81.5	67.3
DSAN [34]	54.4	70.8	75.4	60.4	67.8	68.0	62.6	<b>55.9</b>	78.5	<b>73.8</b>	<b>60.6</b>	<b>83.1</b>	67.6
TADA [39]	53.1	72.3	77.2	59.1	71.2	72.1	59.7	53.1	78.4	72.4	60.0	82.9	67.6
DMP [5]	52.3	73.0	77.3	64.3	72.0	71.8	63.6	52.7	78.5	72.0	57.7	81.6	68.1
ATM [52]	52.4	72.6	80.2	61.1	72.0	72.6	59.5	52.0	79.1	73.3	58.9	83.4	67.9
<b>DoTNet</b>	52.9	<b>75.2</b>	80.2	<b>66.0</b>	<b>77.7</b>	<b>78.9</b>	<b>66.0</b>	50.5	<b>82.0</b>	68.4	51.2	82.0	<b>69.3</b>

regions by incorporating region-wise domain discriminator. Thus, it improves the mean accuracy to 88.4%. Different from TADA, DoTNet learns transferable features by mapping the source samples into the target domain through the domain-level attention, and it obtains the highest accuracy 89.5%. Note that all the methods perform well on tasks **D→W** and **W→D** since there is a smaller domain discrepancy between **D** (high-quality images) and **W** (low-quality images) than others. Though the results of DoTNet are not the best on tasks **D→W** and **W→D**, it consistently outperforms all competitors on the remaining tasks. Note also that domain **A** consists of images from online merchants, domains **D** and **W** consist of different quality images from a realistic office or home environment. This domain discrepancy (virtual-to-real) puts forward greater demands on the generalization ability of features. As shown in the table, tasks **D→A** and **W→A** are common difficulties for all methods. We see that DoTNet achieves the best accuracies 75.8% and 75.0% on these two tasks, respectively. These results validate that modeling sample correspondence across domains through the domain-level attention is effective for reducing domain discrepancy.

The results of Office-Home are shown in Table 2. There are more object classes in Office-Home than other datasets, which brings larger challenge to UDA methods. On the one hand, DANN learns domain-invariant features in the adver-

sarial training mechanism, and its mean accuracy is 56.3%. CDAN+E extends DANN by introducing label information into the adversarial training process and improves mean accuracy to 65.8%. On the other hand, KGOT exploits OT in kernel space and then obtains its average accuracy 54.7%, while DeepJDOT and ETD achieve mean accuracies of 64.3% and 67.3%, respectively. These results empirically demonstrate that discriminative features are vital for enhancing the classification performance on datasets with large-scale classes. Our DoTNet improves the performance on most transfer tasks and achieves the highest average accuracy 69.3%. Note that the accuracy of DoTNet is 1.7% higher than that of DSAN, which reduces the domain discrepancy in a class-wise manner. Though CKB explicitly characterizes the class-conditional distribution discrepancy, its accuracy is lower than that of DoTNet by 0.8%. The superiority of DoTNet over these methods can be attributed to empirical results that utilization of the pseudo-labels increases prediction uncertainty for classification methods. Technically, our DoTNet models sample correspondence and projects source samples into the target domain via the domain-level attention, and then it enhances the intra-class compactness and inter-class separability via local structure regularization. This new method learns transferable features without suffering from the additional risk brought by pseudo-labels.

VisDA-2017 is a challenging dataset since there exists

TABLE 3  
Accuracies (%) on VisDA-2017 (ResNet-101).

VisDA-2017	plane	bicycl	bus	car	horse	knife	mcycl	person	plant	sktbrd	train	truck	Mean
Source-Only [50]	72.3	6.1	63.4	91.7	52.7	7.9	80.1	5.6	90.1	18.5	78.1	25.9	49.4
DAN [3]	68.1	15.4	76.5	87.0	71.1	48.9	82.3	51.5	88.7	33.2	88.9	42.2	62.8
DANN [10]	81.9	77.7	82.8	44.3	81.2	29.5	65.1	28.6	51.9	54.6	82.8	7.8	57.4
CDAN [20]	85.2	66.9	<b>83.0</b>	50.8	84.2	74.9	88.1	74.5	83.4	76.0	81.9	38.0	73.9
JAN [18]	75.7	18.7	82.3	86.3	70.2	56.9	80.5	53.8	92.5	32.2	84.5	54.5	65.7
DeepJDOT [14]	85.4	73.4	77.3	87.3	84.1	64.7	91.5	79.3	91.9	44.4	88.5	<b>61.8</b>	77.4
SWD [59]	90.8	82.5	81.7	70.5	91.7	69.5	86.3	77.5	87.4	63.6	85.6	29.2	76.4
CKB [22]	92.5	56.5	<b>83.7</b>	82.4	93.5	85.7	93.5	71.1	93.4	82.7	83.9	18.4	78.1
TPN [35]	93.7	<b>85.1</b>	69.2	81.6	93.5	61.9	89.3	81.4	<b>93.5</b>	81.6	84.5	49.9	80.4
DSAN [34]	90.9	66.9	75.7	62.4	88.9	77.0	<b>93.7</b>	75.1	92.8	67.6	89.1	39.4	75.1
DMP [5]	92.1	75.0	78.9	75.5	91.2	81.9	89.0	77.2	93.3	77.4	84.8	35.1	79.3
ATM [52]	93.9	65.1	<b>83.7</b>	72.1	92.2	<b>92.5</b>	92.4	79.7	86.1	47.8	86.1	22.0	76.1
<b>DoTNet</b>	<b>96.1</b>	81.4	71.1	78.6	<b>94.2</b>	91.2	88.8	<b>85.4</b>	92.3	<b>90.6</b>	<b>92.7</b>	56.4	<b>84.9</b>

class-imbalance and large virtual-to-real domain discrepancy simultaneously. The accuracies of each class and mean accuracy are shown in Table 3. Specifically, the mean accuracy is derived from the average of all class-wise accuracies, and it is used to measure the overall performance of a specified UDA method. We can see that *truck* is a common barrier for all the methods to achieve better mean accuracies. DeepJDOT performs best on the *truck* class while the mean accuracy is only 77.4%. Perhaps the class-imbalance problem disturbs its optimal transport map in the joint space of features and class labels. DoTNet achieves rank-2 accuracy in the *truck* class and has better performance than other methods. It indicates that achievement of local semantic consistency without utilizing pseudo-labels is reliable in dealing with the class-imbalance problem. TPN simultaneously optimizes domain discrepancy and prototype-based class-wise domain discrepancy, and DMP learns the discriminative structure of target domains through a manifold metric alignment. The mean accuracies of TPN and DMP are relatively close. We see that DoTNet outperforms all the remaining methods with the highest mean accuracy 84.9%, which is 4.5% and 5.6% higher than TPN and DMP, respectively. These results indicate that DoTNet is good at capturing sample correspondence and learns transferable features even when the domain discrepancy is large.

accuracy decreases slowly among the peak area, which validate that our model DoTNet is rather stable under different parameter values of the local structure regularization.

TABLE 4  
Accuracies (%) of ablation study.

Att.	$\mathcal{L}_s$	$\mathcal{L}_t$	$\mathcal{L}_{ent}$	ImageCLEF		VisDA-2017	Office-31	
				C→I	I→C	S→R	A→W	W→A
DA				92.8	96.0	81.4	90.7	73.4
DA	✓			94.3	97.3	82.5	93.0	74.4
DA		✓	✓	94.7	97.3	83.3	93.8	73.9
DA	✓	✓	✓	<b>95.3</b>	<b>97.8</b>	<b>84.9</b>	<b>94.6</b>	<b>75.0</b>
PA	✓	✓	✓	93.7	96.8	68.8	85.5	69.4

**Ablation Study.** The overall objective function of DoTNet can be decomposed into three parts, i.e., the cross-entropy term  $\mathcal{L}_{tce}$  based on the domain-level attention, the supervised local structure learning term  $\mathcal{L}_s$ , and the unsupervised local structure learning terms  $\mathcal{L}_t$  and  $\mathcal{L}_{ent}$ . To explore the impacts of these parts, we conduct ablation study and show the results in Table 4. We notice that  $\mathcal{L}_{tce}$  has been replaced by *Att.* (Attention), with the aim to further distinguish the patch-level attention (PA) in standard Transformers and our domain-level attention (DA).

The accuracies shown in the first row indicate that the domain-level attention, which is implemented via the cross-entropy term  $\mathcal{L}_{tce}$ , nearly achieves SOTA performance. These results validate the theoretical connection, as shown in Section 3.2, that our domain-level attention module is helpful to reduce domain discrepancy. Notice that both the supervised structure learning strategy (with  $\mathcal{L}_s$ ) and the unsupervised strategy (with  $\mathcal{L}_t$  and  $\mathcal{L}_{ent}$ ) can improve the basic model using  $\mathcal{L}_{tce}$  only. We also see that DoTNet with all the loss terms consistently achieves the best performance. It suggests that the local structure regularization terms of the two domains provide substantial advantages in learning transferable and discriminative features.

To further study the effectiveness of the domain-level attention, we design the PA module to replace DA. Specifically, PA employs a single-head attention and regards each element of the given feature vectors as a patch with spatial size  $1 \times 1$ . For fair comparison, we implement PA with the same architecture as the domain-specific projections in DoT. The results are also shown in Table 4. We see that the PA module with the locality regularization terms performs

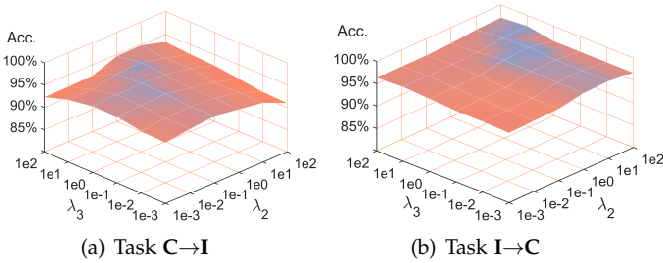


Fig. 3. Hyper-parameter sensitivity of  $\lambda_2$  and  $\lambda_3$  on ImageCLEF-DA.

**Parameter Sensitivity.** We investigate the selection of hyper-parameters  $\lambda_2$  and  $\lambda_3$  on ImageCLEF-DA tasks  $C \rightarrow I$  and  $I \rightarrow C$ . The parameters  $\lambda_2$  and  $\lambda_3$  act on the local structure regularization, where the former balances the source locality preserving loss  $\mathcal{L}_s$  and the latter works on the target locality preserving loss  $\mathcal{L}_t$ . The parameters  $\lambda_2$  and  $\lambda_3$  are searched from  $\{1e-3, 1e-2, 1e-1, 1e0, 1e1, 1e2\}$ . The grid search results are shown in Figure 3. We can see that the



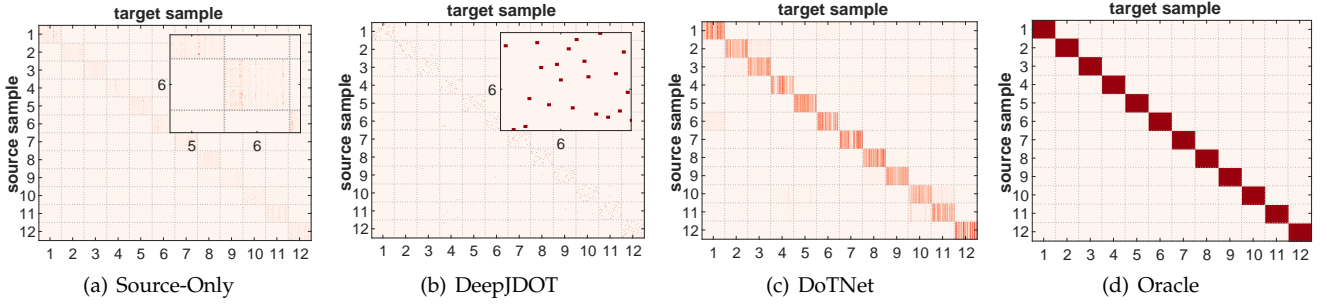


Fig. 4. The heat-maps of attention matrices or optimal transport plan  $\gamma^*$  on ImageCLEF task  $I \rightarrow C$ . Specifically, (a) and (c) are based on the attention matrices of Source-Only and our DoTNet models, respectively. (b) is the visualization of the optimal transport plan  $\gamma^*$  obtained from DeepJDOT. The Oracle (d) is the heat-map of attention matrix computed by the ground-truth labels. Best viewed in color.

well on ImageCLEF but poorly on more challenging Office-31 and VisDA-2017 datasets. However, DoT consistently outperforms the new combination manner, even with a large margin on more challenging tasks. It validates the superiority of the domain-level attention over the patch-level attention in dealing with UDA problems.

**Local Semantic Consistency.** To further explore the relationship between the transformed source samples with the semantic relevant target samples, we utilize heat-map to visualize the attention matrices of Source-Only, DeepJDOT, DoTNet and Oracle for ImageCLEF-DA task  $I \rightarrow C$  in Figure 4. Specifically, we regard the optimal transport plan  $\gamma$  of DeepJDOT as the attention matrix. For Oracle, if the ground-truth labels of the source and target samples are the same, the corresponding entry of the attention matrix equals to 1, otherwise, it is 0. Then, the non-zero elements of each row will be normalized. The Oracle case in Figure 4(d) suggests that if each transformed source sample is a weighted sum of the target samples within the same class, the heat-map is diagonal colored. We can observe from Figure 4(a) that the Source-Only model does not allow relational inference between source and target samples. The optimal transport plan  $\gamma$  is a sparse matrix with row-sum and column-sum equal the marginal distributions. For DeepJDOT, the related sample-pairs will have a higher weight in  $\gamma$ , which is shown in Figure 4(b). Differently, the domain-level attention of DoTNet increases normalization on the row of the attention matrix, which aims to find more relevant target samples to obtain the transformed source sample. With the help of the structure learning strategy, DoTNet achieves a local semantic consistency across domains as shown in Figure 4(c). Though there is still room for improvement compared with the Oracle case in Figure 4(d), DoTNet has achieved the class-wise domain alignment without utilizing the soft labels or pseudo-labels of the uncertain target samples.

**Domain Correlation.** In statistics, the cross-covariance matrix measures the correlation degree between two random variables with multiple dimensions. Mathematically, the cross-covariance matrix  $\Sigma_{F^s F^t}$  is estimated by  $\mathbb{E}[(F^s - \mathbb{E}[F^s])(F^t - \mathbb{E}[F^t])^T]$ , and similarly for  $\Sigma_{\hat{F}^s F^t}$ . Here, we compute  $\Sigma_{F^s F^t}$  based on features  $F^s$  and  $F^t$  from Source-Only, and obtain  $\Sigma_{\hat{F}^s F^t}$  based on the features  $\hat{F}^s$  and  $F^t$  from DoT. We compute the Frobenius-norm (F-norm) of the cross-covariance matrices to compare the dependency between the learned domain-invariant features. Generally,

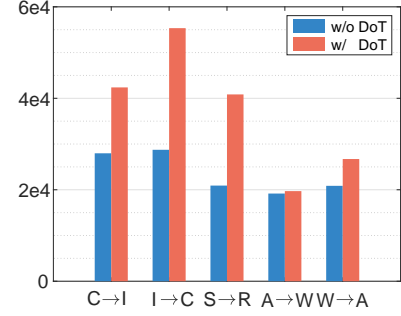


Fig. 5. F-norm of the cross-covariance matrix based on the embedded features. Best viewed in color.

the F-norm characterizes global correlation degree for the cross-covariance matrix. A larger norm indicates a larger correlation degree between the source and target domains.

The experiments are conducted on ImageCLEF-DA tasks ( $C \rightarrow I$  and  $I \rightarrow C$ ), VisDA-2017 task ( $S \rightarrow R$ ), and Office-31 tasks ( $A \rightarrow W$  and  $W \rightarrow A$ ). As shown in Figure 5, we denote  $\|\Sigma_{F^s F^t}\|_F$  as w/o DoT and  $\|\Sigma_{\hat{F}^s F^t}\|_F$  as w/ DoT. We see that DoT has larger F-norms on all of these UDA tasks. It means that the sample correlations across different domains are improved. By considering the classification performance obtained by DoT, we think the larger norms are closely related to the model's generalization ability. This is consistent with the empirical results and important conclusions shown by Xu *et al.* [51]. In other words, the results validate that DoT achieves domain alignment and then improves the mode's generalization performance by capturing the sample correspondence between domains.

**Wasserstein Metric.** In Section 3.3, we establish the estimation error and generalization bound based on  $\mathcal{W}_2$ -distance. To verify the rationality and effectiveness of these theoretical results, the  $\mathcal{W}_2$ -distance is calculated for the features obtained by several different methods and then presented in Figure 7. Specifically, task  $I \rightarrow C$  of ImageCLEF and task  $S \rightarrow R$  of visda-2017 are still used for simplicity. The features obtained by DeepJDOT, ATM and DoTNet are input into the Sink-horn's iterative algorithm, respectively, and then the  $\mathcal{W}_2$ -distances are obtained. We can see that in both learning tasks, the  $\mathcal{W}_2$ -distance of DoTNet is smaller than that obtained by the other two methods, i.e., DeepJDOT and ATM, and the comparison on  $S \rightarrow R$  task is



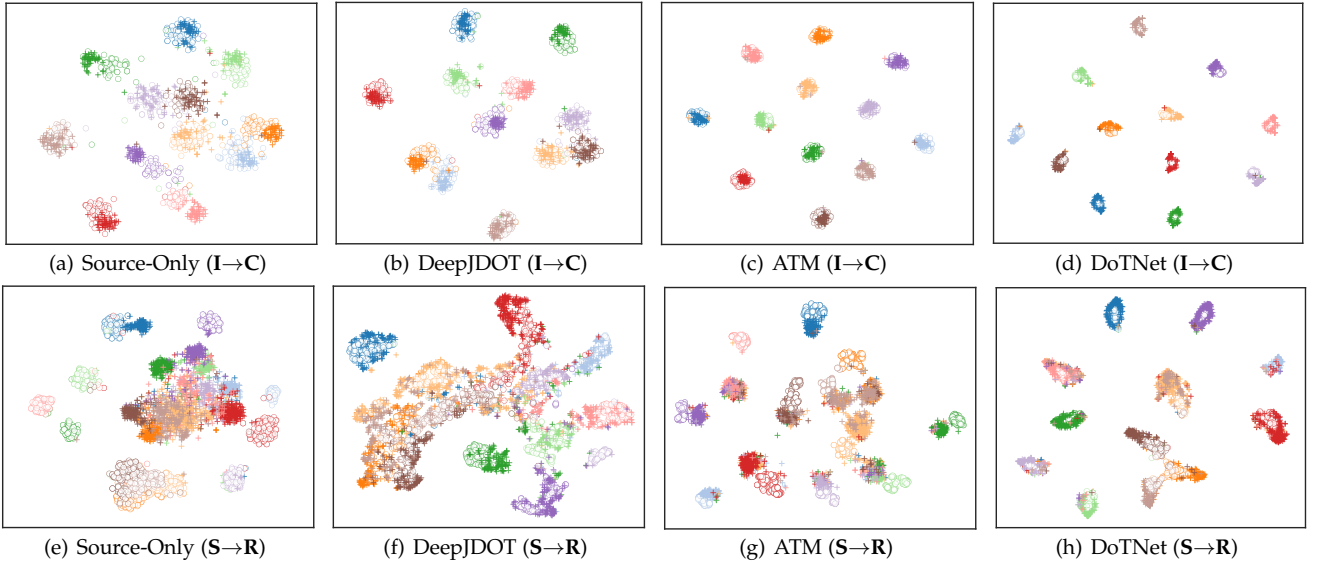


Fig. 6. The t-SNE visualization of features generated by Source-Only, DeepJDOT, ATM and DoTNet on ImageCLEF task  $I \rightarrow C$  and VisDA-2017 task  $S \rightarrow R$ , respectively. Here, “o” means source domain and “+” means target domain. Each color denotes one class. Best viewed in color.

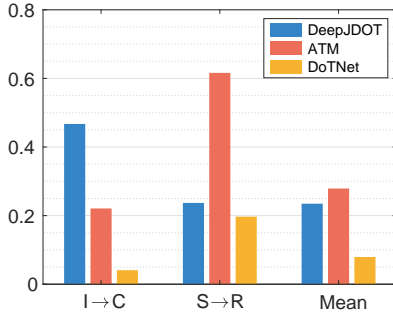


Fig. 7.  $\mathcal{W}_2$ -distance between the source domain and the target domain.

more obvious. “Mean” represents the average  $\mathcal{W}_2$ -distance corresponding to two groups of tasks, and DoTNet still keeps the superiority on distance value. Figure 7 shows that DoTNet effectively reduces the domain discrepancy without introducing the complex iteration computation. It also verifies the effectiveness of the learning theory and model based on the  $\mathcal{W}_2$ -distance again.

**Feature Visualization.** To provide an intuitive understanding of the aligned features, we use t-distribution Stochastic Neighbour Embedding (t-SNE) [60] to visualize the features obtained by different methods. We conduct this experiment on ImageCLEF-DA task  $I \rightarrow C$  and VisDA-2017 task  $S \rightarrow R$ . For VisDA-2017, we randomly selected 2000 samples across 12 categories from the source and target domains according to the original category ratio. The results are shown in Figure 6. Compared with DeepJDOT and ATM, our DoTNet achieves better intra-class compactness since samples with the same class are closer. In Figure 6(e), the source features have an obvious discriminative structure while the target features collide into a mess due to the large synthetic-to-real domain gap in VisDA-2017. DeepJDOT achieves a pair-wise matching across domains by seeking an optimal transport plan  $\gamma$  in the joint space. However, in Figure 6(f), some aligned classes are not separable with

a large margin. Figure 6(g) further indicates that the Maximum Density Divergence (MDD) loss guarantees ATM to learn discriminative features. In Figure 6(h), we can observe that DoTNet matches the complex structures of the source and target domains along with achieving the intra-class compactness on the target domain.

**Scatter Analysis.** DoT learns transferable features by capturing sample correspondence, rather than explicitly modeling domain discrepancy. To further verify that DoT also brings domain alignment, we measure four kinds of distances between the transformed source domain and target domain in the training process, i.e., within-class scatter, between-class scatter, SrcMean-to-TarMean and  $\mathcal{W}_2$ -distance. Within-class scatter denotes the mean Euclidean distance between all samples and their corresponding class center. Between-class scatter computes the mean Euclidean distance between all class centers and the domain center, which is the average over samples from the transformed source domain and target domain. SrcMean-to-TarMean is the mean Euclidean distance between the source class centers and the target class centers.  $\mathcal{W}_2$ -distance is the 2-Wasserstein distance in the feature space.

Figure 8 shows the four distances on ImageCLEF-DA task  $I \rightarrow C$  and VisDA-2017 task  $S \rightarrow R$ , respectively. In Figure 8(a), we can observe that the target domain has a much larger within-class scatter than the transformed source domain at first, and then reduces to 0, which suggests that DoT brings intra-class compactness. The between-class scatter of the target domain in Figure 8(b) is firstly much lower than that of the labeled transformed source domain, and then stabilizes at a high-level along with the training process, indicating that DoT achieves a large inter-class separability. The decreasing SrcMean-to-TarMean distance in Figure 8(c) verifies that the local semantic consistency of DoT enhances the class-wise domain alignment. The gradually decreasing  $\mathcal{W}_2$ -distance in Figure 8(d) demonstrates that DoT minimizes the generalization upper bound with the empirical Wasserstein distance. Similar curves are shown in Figure 8(e)-(h) on the

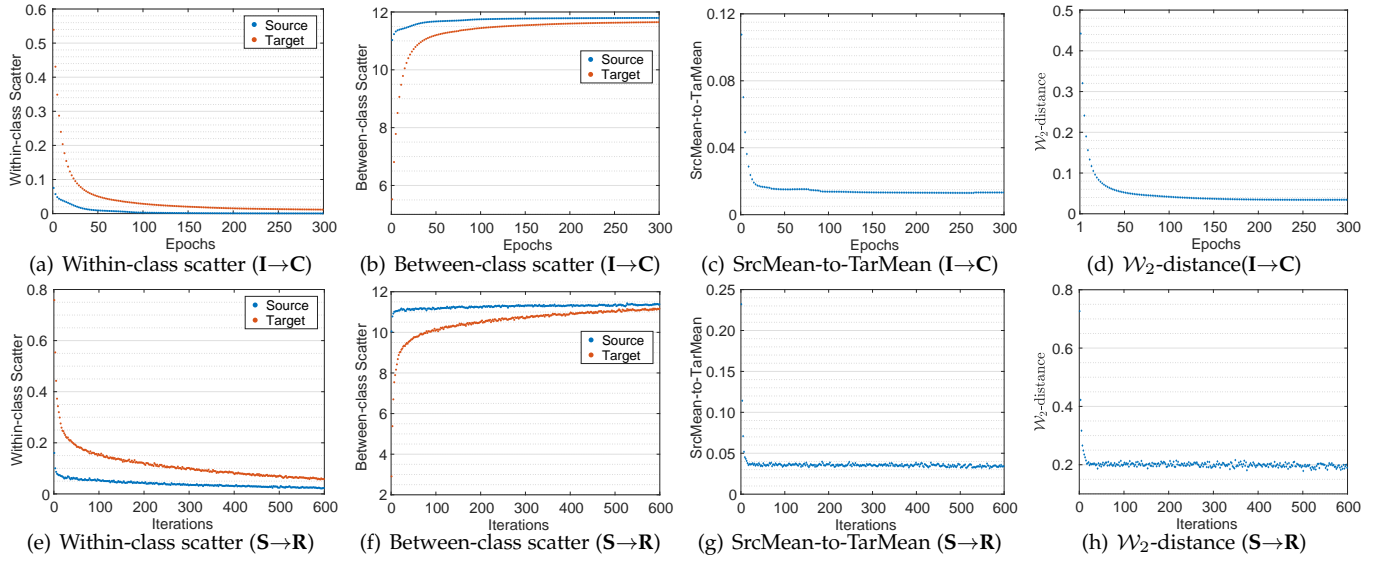


Fig. 8. Scatter analysis for the embedded features on ImageCLEF-DA task  $I \rightarrow C$  and VisDA-2017 task  $S \rightarrow R$ .  $\hat{F}^s$  is used for the source domain, and  $\hat{F}^t$  for the target domain. Best viewed in color.

$S \rightarrow R$  task. Generally speaking, all these results indicate that DoT successfully learns the local semantic consistency with domain-level attention mechanism.

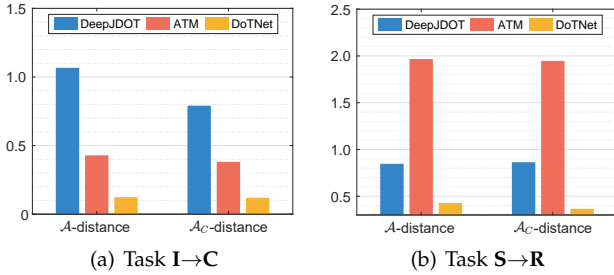


Fig. 9.  $\mathcal{A}$ -distance and  $\mathcal{A}_C$ -distance for ImageCLEF-DA task  $I \rightarrow C$  and VisDA-2017 task  $S \rightarrow R$ . Best viewed in color.

**Domain Discrepancy.** Inspired by the pioneering work [6],  $\mathcal{A}$ -distance have been widely used to measure domain discrepancy. The  $\mathcal{A}$ -distance is estimated by  $d_{\mathcal{A}} = 2(1 - 2\varepsilon)$ , where  $\varepsilon$  denotes the test error of a classifier trained for distinguishing the source and target domains. Thus, the smaller  $\mathcal{A}$ -distance, the better global domain alignment. To measure class-wise domain discrepancy, we estimate  $\mathcal{A}_C$ -distance by  $d_{\mathcal{A}_C} = \mathbb{E}[d_{\mathcal{A}_c}]$ , where  $d_{\mathcal{A}_c}$  is the  $\mathcal{A}$ -distance for samples from the same class but different domains, and  $\mathbb{E}[\cdot]$  is the expectation on target domain. The smaller  $\mathcal{A}_C$ -distance, the better class-wise domain alignment. We provide the  $\mathcal{A}$ -distance and  $\mathcal{A}_C$ -distance of DeepJDOT, ATM and DoTNet on ImageCLEF-DA task  $I \rightarrow C$  and VisDA-2017 task  $S \rightarrow R$ , respectively. As shown in Figure 9, ATM has smaller  $\mathcal{A}$ -distance and  $\mathcal{A}_C$ -distance than DeepJDOT on task  $I \rightarrow C$  while contrary performance on task  $S \rightarrow R$ . We also note that DoTNet achieves the smallest  $\mathcal{A}$ -distance and  $\mathcal{A}_C$ -distance on both tasks, which validates the effectiveness of DoTNet in reducing domain discrepancy. Additionally,  $\mathcal{A}_C$ -distances are frequently smaller than  $\mathcal{A}$ -distances. This can be attributed to the local semantic consistency learned by the domain-level attention in DoTNet.

## 5 CONCLUSION

In this paper, we propose a novel method called Domain-transformer (DoT) for unsupervised domain adaptation. We define the domain-level attention based on the key component of the Transformer, i.e., the cross-attention mechanism. Instead of replacing the CNN-backbones with a pure transformer architecture, DoT integrates the domain-level attention with the prominent CNN-backbones in computer vision to deal with UDA. With the help of domain structure learning strategy, DoT achieves discriminative feature extraction and transfer across domains. From the perspective of Wasserstein geometry and statistical learning theory, we connect the domain-level attention with the optimal transport algorithm and derive a generalization error bound with Wasserstein metric. By virtue of the OT-like map, DoT not only ensures the local semantic consistency of representations, but also avoids explicit divergence optimization. In our future work, we will give more thinking about how to employ the merits of the transformers on more general problems including meta learning.

## REFERENCES

- [1] S. J. Pan and Q. Yang, "A survey on transfer learning," *IEEE TKDE*, vol. 22, no. 10, pp. 1345–1359, 2009.
- [2] N. Courty, R. Flamary, D. Tuia, and A. Rakotomamonjy, "Optimal transport for domain adaptation," *IEEE TPAMI*, vol. 39, no. 9, pp. 1853–1865, 2016.
- [3] M. Long, Y. Cao, Z. Cao, J. Wang, and M. I. Jordan, "Transferable representation learning with deep adaptation networks," *IEEE TPAMI*, vol. 41, no. 12, pp. 3071–3085, 2019.
- [4] X. Yang, C. Deng, T. Liu, and D. Tao, "Heterogeneous graph attention network for unsupervised multiple-target domain adaptation," *IEEE TPAMI*, 2020, accept.
- [5] Y. W. Luo, C. X. Ren, D. Q. Dai, and H. Yan, "Unsupervised domain adaptation via discriminative manifold propagation," *IEEE TPAMI*, vol. 44, no. 3, pp. 1653–1669, 2022.
- [6] S. Ben-David, J. Blitzer, K. Crammer, A. Kulesza, F. Pereira, and J. W. Vaughan, "A theory of learning from different domains," *Machine learning*, vol. 79, no. 1-2, pp. 151–175, 2010.
- [7] S. J. Pan, I. W. Tsang, J. T. Kwok, and Q. Yang, "Domain adaptation via transfer component analysis," *IEEE TNN*, vol. 22, no. 2, pp. 199–210, 2010.

- [8] B. Sun, J. Feng, and K. Saenko, "Return of frustratingly easy domain adaptation," in *AAAI*, 2016, pp. 2058–2065.
- [9] B. Gong, Y. Shi, F. Sha, and K. Grauman, "Geodesic flow kernel for unsupervised domain adaptation," in *CVPR*, 2012, pp. 2066–2073.
- [10] Y. Ganin, E. Ustinova, H. Ajakan, P. Germain, H. Larochelle, F. Laviolette, M. Marchand, and V. Lempitsky, "Domain-adversarial training of neural networks," *JMLR*, vol. 17, no. 1, pp. 2096–2030, 2016.
- [11] E. Tzeng, J. Hoffman, K. Saenko, and T. Darrell, "Adversarial discriminative domain adaptation," in *CVPR*, 2017, pp. 7167–7176.
- [12] C. X. Ren, B. H. Liang, P. Ge, Y. M. Zhai, and Z. Lei, "Domain adaptive person re-identification via camera style generation and label propagation," *IEEE TIFS*, vol. 15, pp. 1290–1302, 2020.
- [13] Z. Zhang, M. Wang, and A. Nehorai, "Optimal transport in reproducing kernel hilbert spaces: Theory and applications," *IEEE TPAMI*, vol. 42, no. 7, pp. 1741–1754, 2019.
- [14] B. Bhushan Damodaran, B. Kellenberger, R. Flamary, D. Tuia, and N. Courty, "Deepjdot: Deep joint distribution optimal transport for unsupervised domain adaptation," in *ECCV*, 2018, pp. 447–463.
- [15] M. X. Li, Y. M. Zhai, Y. W. Luo, P. Ge, and C. X. Ren, "Enhanced transport distance for unsupervised domain adaptation," in *CVPR*, 2020, pp. 13936–13944.
- [16] K. Zhang, B. Schölkopf, K. Muandet, and Z. Wang, "Domain adaptation under target and conditional shift," in *ICML*, 2013, pp. 819–827.
- [17] R. Tachet des Combes, H. Zhao, Y.-X. Wang, and G. Gordon, "Domain adaptation with conditional distribution matching and generalized label shift," in *NeurIPS*, 2020.
- [18] M. Long, Y. Cao, J. Wang, and M. Jordan, "Deep transfer learning with joint adaptation networks," in *ICML*, 2017, pp. 2208–2217.
- [19] H. Yan, Y. Ding, P. Li, Q. Wang, Y. Xu, and W. Zuo, "Mind the class weight bias: Weighted maximum mean discrepancy for unsupervised domain adaptation," in *CVPR*, 2017, pp. 2272–2281.
- [20] M. Long, Z. Cao, J. Wang, and M. Jordan, "Conditional adversarial domain adaptation," in *NeurIPS*, 2018, pp. 1640–1650.
- [21] N. Courty, R. Flamary, A. Habrard, and A. Rakotomamonjy, "Joint distribution optimal transportation for domain adaptation," in *NeurIPS*, 2017, pp. 3733–3742.
- [22] Y. W. Luo and C. X. Ren, "Conditional bures metric for domain adaptation," in *CVPR*, 2021, pp. 13989–13998.
- [23] A. Vaswani, N. Shazeer, N. Parmar, J. Uszkoreit, L. Jones, A. N. Gomez, L. Kaiser, and I. Polosukhin, "Attention is all you need," in *NeurIPS*, 2017, pp. 5998–6008.
- [24] A. Dosovitskiy, L. Beyer, A. Kolesnikov, D. Weissenborn, X. Zhai, T. Unterthiner, M. Dehghani, M. Minderer, G. Heigold, S. Gelly, J. Uszkoreit, and N. Houlsby, "An image is worth 16x16 words: Transformers for image recognition at scale," in *ICLR*, 2021.
- [25] K. He, X. Zhang, S. Ren, and J. Sun, "Deep residual learning for image recognition," in *CVPR*, 2016, pp. 770–778.
- [26] H. Touvron, M. Cord, M. Douze, F. Massa, A. Sablayrolles, and H. Jegou, "Training data-efficient image transformers & distillation through attention," in *ICML*, 2021, pp. 10347–10357.
- [27] W. Wang, E. Xie, X. Li, D.-P. Fan, K. Song, D. Liang, T. Lu, P. Luo, and L. Shao, "Pyramid vision transformer: A versatile backbone for dense prediction without convolutions," in *ICCV*, 2021, pp. 568–578.
- [28] Z. Liu, Y. Lin, Y. Cao, H. Hu, Y. Wei, Z. Zhang, S. Lin, and B. Guo, "Swin transformer: Hierarchical vision transformer using shifted windows," in *ICCV*, 2021, pp. 10012–10022.
- [29] C. Chen, Q. Fan, and R. Panda, "Crossvit: Cross-attention multi-scale vision transformer for image classification," *arXiv preprint arXiv:2103.14899*, 2021.
- [30] Y. Chen, S. Gong, and L. Bazzani, "Image search with text feedback by visiolinguistic attention learning," in *CVPR*, 2020, pp. 3001–3011.
- [31] Y. LeCun, Y. Bengio et al., "Convolutional networks for images, speech, and time series."
- [32] C. X. Ren, D. Q. Dai, X. He, and H. Yan, "Sample weighting: an inherent approach for outlier suppressing discriminant analysis," *IEEE TKDE*, vol. 27, no. 11, pp. 3070–3083, 2015.
- [33] C. X. Ren, X. Xu, and H. Yan, "Generalized conditional domain adaptation: A causal perspective with low-rank translators," *IEEE TCYB*, vol. 50, no. 2, pp. 821–834, 2018.
- [34] Y. Zhu, F. Zhuang, J. Wang, G. Ke, J. Chen, J. Bian, H. Xiong, and Q. He, "Deep subdomain adaptation network for image classification," *IEEE TNNLS*, 2020.
- [35] Y. Pan, T. Yao, Y. Li, Y. Wang, C.-W. Ngo, and T. Mei, "Transferrable prototypical networks for unsupervised domain adaptation," in *CVPR*, 2019, pp. 2239–2247.
- [36] M. Zaheer, G. Guruganesh, K. A. Dubey, J. Ainslie, C. Alberti, S. Ontanon, P. Pham, A. Ravula, Q. Wang, L. Yang, and A. Ahmed, "Big bird: Transformers for longer sequences," in *NeurIPS*, 2020, pp. 17283–17297.
- [37] Y. Li, K. Zhang, J. Cao, R. Timofte, and L. Van Gool, "Localvit: Bringing locality to vision transformers," *arXiv preprint arXiv:2104.05707*, 2021.
- [38] X. Zhu, W. Su, L. Lu, B. Li, X. Wang, and J. Dai, "Deformable detr: Deformable transformers for end-to-end object detection," in *ICLR*, 2021.
- [39] X. Wang, L. Li, W. Ye, M. Long, and J. Wang, "Transferable attention for domain adaptation," in *AAAI*, 2019, pp. 5345–5352.
- [40] W. Ma, J. Zhang, S. Li, C. H. Liu, Y. Wang, and W. Li, "Exploiting both domain-specific and invariant knowledge via a win-win transformer for unsupervised domain adaptation," *arXiv preprint arXiv:2111.12941*, 2021.
- [41] J. Yang, J. Liu, N. Xu, and J. Huang, "Tvt: Transferable vision transformer for unsupervised domain adaptation," *arXiv preprint arXiv:2108.05988*, 2021.
- [42] G. Yang, H. Tang, Z. Zhong, M. Ding, L. Shao, N. Sebe, and E. Ricci, "Transformer-based source-free domain adaptation," *arXiv preprint arXiv:2105.14138*, 2021.
- [43] M. Cuturi, "Sinkhorn distances: Lightspeed computation of optimal transport," in *NeurIPS*, 2013, pp. 2292–2300.
- [44] Q. Wang, X. He, X. Jiang, and X. Li, "Robust bi-stochastic graph regularized matrix factorization for data clustering," *IEEE TPAMI*, vol. 44, no. 1, pp. 390–403, 2022.
- [45] P. A. Knight, "The sinkhorn-knopp algorithm: convergence and applications," *SIAM Journal on Matrix Analysis and Applications*, vol. 30, pp. 261–275, 2008.
- [46] C. Villani, *Optimal transport: old and new*. Springer, 2009.
- [47] B. K. Sriperumbudur, K. Fukumizu, A. Gretton, B. Schölkopf, and G. R. Lanckriet, "On integral probability metrics,  $\phi$ -divergences and binary classification," *arXiv:0901.2698*, 2009.
- [48] G. Peyré, M. Cuturi et al., "Computational optimal transport: With applications to data science," *Foundations and Trends® in Machine Learning*, vol. 11, no. 5-6, pp. 355–607, 2019.
- [49] X. He and P. Niyogi, "Locality preserving projections," in *NeurIPS*, 2003, pp. 153–160.
- [50] K. He, X. Zhang, S. Ren, and J. Sun, "Deep residual learning for image recognition," in *CVPR*, 2016, pp. 770–778.
- [51] R. Xu, G. Li, J. Yang, and L. Lin, "Larger norm more transferable: An adaptive feature norm approach for unsupervised domain adaptation," in *ICCV*, 2019, pp. 1426–1435.
- [52] J. Li, E. Chen, Z. Ding, L. Zhu, K. Lu, and H. T. Shen, "Maximum density divergence for domain adaptation," *IEEE TPAMI*, vol. 43, pp. 3918–3930, 2021.
- [53] B. Caputo, H. Müller, J. Martinez-Gomez, M. Villegas, B. Acar, N. Patricia, N. Marvasti, S. Üsküdarlı, R. Paredes, M. Cazorla et al., "Imageclef 2014: Overview and analysis of the results," in *International Conference of the Cross-Language Evaluation Forum for European Languages*, 2014, pp. 192–211.
- [54] K. Saenko, B. Kulis, M. Fritz, and T. Darrell, "Adapting visual category models to new domains," in *ECCV*, 2010, pp. 213–226.
- [55] H. Venkateswara, J. Eusebio, S. Chakraborty, and S. Panchanathan, "Deep hashing network for unsupervised domain adaptation," in *CVPR*, 2017, pp. 5018–5027.
- [56] X. Peng, B. Usman, N. Kaushik, J. Hoffman, D. Wang, and K. Saenko, "Visda: The visual domain adaptation challenge," *arXiv preprint arXiv:1710.06924*, 2017.
- [57] T.-Y. Lin, M. Maire, S. Belongie, J. Hays, P. Perona, D. Ramanan, P. Dollár, and C. L. Zitnick, "Microsoft coco: Common objects in context," in *ECCV*, 2014, pp. 740–755.
- [58] O. Russakovsky, J. Deng, H. Su, J. Krause, S. Satheesh, S. Ma, Z. Huang, A. Karpathy, A. Khosla, M. Bernstein et al., "Imagenet large scale visual recognition challenge," *IJCV*, vol. 115, no. 3, pp. 211–252, 2015.
- [59] C. Lee, T. Batra, M. H. Baig, and D. Ulbricht, "Sliced wasserstein discrepancy for unsupervised domain adaptation," in *CVPR*, 2019, pp. 10285–10295.
- [60] L. v. d. Maaten and G. Hinton, "Visualizing data using t-sne," *JMLR*, vol. 9, no. Nov, pp. 2579–2605, 2008.